

The Pennsylvania State University
Schreyer Honors College

Department of Engineering Science and Mechanics

Realization of porous SiO₂ nanoparticles for analyte sensing in the brain

Alessandro Ascani Orsini

May 2023

Review and approved* by the following:

Bruce J. Gluckman

Director of the Centre for Neural Engineering
Professor of Engineering Sciences and Mechanics,
Biomedical Engineering,
Neurosurgery
Thesis Supervisor and Honors Advisor

James H. Adair

Professor of Material Sciences and Engineering,
Biomedical Engineering,
Pharmacology
Thesis Advisor

Mark W. Horn

Professor of Engineering Sciences and Mechanics
Faculty reader

Vincent Meunier

Department Head

P. B. Breneman Chair and Professor of Engineering Science and Mechanics

A thesis submitted in partial fulfillment of the requirements for Baccalaureate degree
in Engineering Science with Honors in Engineering Science.

*Signatures are on file in the Schreyer Honors College.

Abstract

Many diseases affecting the brain have an underlying molecular base that is difficult to study due to the lack of instrumentation with high spatial and temporal resolution. To address this issue we present a study on the fabrication of fluorescent porous silica nanoparticles. These particles aim to restrict the analysis of the system only to the Extracellular Matrix (ECM), reduce the photobleaching rate of the fluorophores, making them last longer and allow the colocalization of multiple dyes permitting in this way to monitor multiple analytes. Starting from the Stöber procedure we used Tetramethylorthosilicate (TMOS) to accelerate the aggregation reaction obtaining highly microporous particles. Based on this revised synthesis we characterized the particles with encapsulated fluorescein, which resulted in leakage of the dye due to its size being very close to the particles' pore diameter. Using a second synthesis to build a shell around the fluorescent particles, we identified the ideal concentration of orthosilicate to use to prevent the leakage and obtain maximum absorbance and emission from the fluorophores. In this way, we developed a probe that can be applied for analyte sensing in the brain. Further testing will be needed to assess the effect of the encapsulation on photobleaching rate and Förster Resonance Energy Transfer (FRET) excitation as well as the integration of the nanoparticles with an external system.

Table of Contents

Acknowledgements	ix
Chapter 1	
Introduction	1
1.1 Problem Statement	1
1.2 Design Needs	1
1.3 Impact	2
1.4 Objective of the Thesis	2
Chapter 2	
Background	3
2.1 Understanding the brain.	3
2.1.1 The structure of the Neuron	3
2.1.2 The Action potential	5
2.1.3 The chemistry behind an action potential.	5
2.1.4 Studying the brain.	7
2.2 Epilepsy	8
2.2.1 Spreading Depolarization	8
2.2.2 Measure Analyte concentrations in the brain	10
2.2.3 Optical probes for Concentration sensing	12
2.2.4 Motivation	12
Chapter 3	
Previous systems	14
3.1 An Optical Endoscope for analyte sensing	14
3.2 Nanoparticles as analyte sensors	15
3.2.1 C-Dots: fluorescent biomarkers Core-shell silica nanoparticles	15
3.2.2 Multiplex analysis probes	17
3.2.3 PSNP - Polystyrene nanoparticles for oxygen sensing	17
3.2.4 PEBBLE nanoparticles - photonic explorer for bioanalysis with biologically localized embedding	18
3.2.5 CPNP - Calcium Phosphate Composite Nanoparticles	18
Chapter 4	
Selection of the dyes	19

4.1	Criteria	20
4.2	A review of O ₂ sensitive fluorophores	21
4.3	A review of K ⁺ sensitive fluorophores	24
4.4	FRET excitation for multiple analyte monitoring	24
Chapter 5		
	Methods and Results	26
5.1	The Stöber procedure	26
5.1.1	Reaction breakdown	27
5.2	Characterization methods	27
5.2.1	Dynamic Light Scattering Analysis	27
5.2.2	BET Analysis	29
5.2.3	BJH Analysis	29
5.2.4	UV-Vis absorbance analysis	29
5.2.5	Emission Analysis	31
5.2.6	SEM	31
5.3	Duplicating the reaction	32
5.4	Identifying the ideal concentrations	33
5.5	Adding porosity to the particles	33
5.5.1	Optimization of the porosity	33
5.6	Encapsulation of fluorophore	37
5.6.1	Absorbance Analysis	39
5.6.1.1	Determining the concentration of fluorophore	40
5.6.2	Results of the encapsulation	40
5.6.3	Double encapsulations	40
Chapter 6		
	Discussion	46
6.1	Advantages compared to previous systems	47
6.2	Impact	48
6.2.1	Economic / Manufacturability / Technology Transfer	48
6.2.2	Environmental/ Sustainability	48
6.2.3	Ethical	48
6.2.4	Health and Safety	48
6.2.5	Social / Political / Global	48
6.3	Optimization and Future Direction	49
Chapter 7		
	Conclusion	50
Appendices		
51		
Chapter A		
	Codes	51

List of Figures

2.1	The structure of the neuron	4
2.2	The axon's membrane modelled as an electrical circuit.	6
2.3	The action potential and sequential conductance of voltage gated Na^+ and K^+ channels.	8
2.4	First evidence of Spreading depression	9
2.5	Effects of Spreading Depolarization on the Action Potential	11
3.1	Optic endoscope for localized analyte monitoring system breakdown	16
4.1	Basic concepts for FRET excitation	25
5.1	Particle size of silica nanoparticles for TEOS 0.28 M based on concentration in H_2O and NH_3	28
5.2	BET Isotherm Linear Plot for highest porosity sample at 75% TMOS	30
5.3	Size of 300 nm silica nanoparticles at different concentrations of H_2O and NH_3 with the difference in size for high and low concentration of NH_4OH	34
5.4	Chemical structures for TMOS and TEOS	35
5.5	Particle properties for different quantities of TMOS and TEOS	36
5.6	SEM images of the particles at different TMOS percentages	38
5.7	Beer-Lambert relationship for fluorescein	39
5.8	Estimated fluorophore concentration in the nanoparticles based on absorbance analysis	42
5.9	Concentration of fluorescein removed over wash	43
5.10	Behaviour of fluorescein in nanoparticles with shells produced over concentrations of orthosilicate	44
5.11	Dynamic Light Scattering analysis of particles size based on shell orthosilicate mixture concentration	45

List of Tables

4.1 Advantages and disadvantages of the main fluorophore groups for Oxygen Sensing	23
--	----

Acknowledgements

First of all, I would like to thank my advisor Dr. Gluckman for taking me into his lab in my first semester of college, guiding, teaching, mentoring and supporting me towards my dream despite the Covid pandemic and all my failed projects.

I would like to express my deepest gratitude to Dr. Adair and Bernie, for their leadership and teaching in these past two years as well as their advising. I learned a lot in such a short amount of time. It was truly a pleasure to work with them.

I want to thank all my professors that through the years contributed to my knowledge, challenged and inspired me to go beyond the concepts taught in class. Especially, I would like to thank Dr. Passmore and Dr. Horn for all their great help in reviewing this thesis and helping me getting it finished. I would like to thank Dr. Gray for his great classes that made me love engineering even more, Dr. Elliott for making me even more passionate in the relationship between neuroscience and engineering, Dr. Das for giving me the passion for nanomaterial and making me understand their true hidden beauty, Dr. Drew for his great guidance in Neuroscience physiology and its connection to engineering and Dr. Kiani for introducing me to the basics of implantable medical devices circuitry, my next field of focus.

I would like to thank Eashan Chopde for working with me on the design of the porous silica nanoparticles and for mentoring me, Rene Gangarosa for the development of the optic endoscope and Keeley Naylor for all the support and help whenever I had questions in lab.

I would like to thank my friends for making this college experience great. Thank you to those that support and believe in me, those who I worked with, before and after covid, watched 'Transistorized' late at night before the ESC312 midterm with, had Starbucks and planned crazy adventures on a daily with and talked in lab or through phone to once in a while. All of this mattered to me, thank you.

Finally, I would like to thank my family that supports me every day and without which I wouldn't have been able to do this wholesome experience and pursue my path. Thank you for bearing with me.

Thank you all for everything, these have been four great years and thanks to all of you I have grown so much and learned even more as a researcher. This is a great milestone towards my dream and I owe it to you.

Chapter 1

Introduction

1.1 Problem Statement

Epilepsy is a common, often debilitating condition affecting the brain. 5.1 million people including adults and children are currently affected by this disease. Often, as a consequence of an epileptic seizure, the patient might also experience a spontaneous phenomenon called *spreading depression*, also known as *spreading depolarization*. This consists in waves of intense neuronal and glial depolarization followed by a subduing of the electrical signal [1]. Both phenomena function by affecting the concentrations of analytes such as Potassium (K^+) or Oxygen (O_2). Thus, having a tool that permits an in-vivo analysis of the concentration for such elements with high spatial and temporal resolution is fundamental to improve our understanding of the brain and its diseases.

1.2 Design Needs

The project develops on two branches: the system and the sensor.

On one side, there is the optimization of a previously developed design by Gangarosa [2] with the addition of further photodiodes to measure multiple concentrations at once as well as calibration and adjustments to make the system compatible with the sensor.

On the other side there is the design and synthesis of the sensor that is going to be connected on the front end of the system and applied to the brain. This part needs to be small and made of a biocompatible material. This element will need to not alter or block the movement of the ions and will have to modulate light based on the concentrations of analyte in the solution with minimum influence by other factors.

The project consists of experimentation in clean laboratory environment with ammonia compounds, orthosilicates, ethanol, volatile organic compounds (VOCs), fiber optic, electronics, centrifuge, scanning electron microscopy (SEM), Brunauer-Emmett-Teller analysis (BET), Barrett-Joyner-Halenda (BJH), absorbance analysis in UV-Vis

and Emission analysis.

1.3 Impact

The implementation of our device would have an impact on society due to the research improvement towards the analysis of many diseases, including epilepsy, migraine but also neurodegenerative diseases such as Alzheimer's. Also it would allow us to have a better understanding of models for small particles in biological systems and in animal models for disease studies that have an effect on ionic balances inside the body.

From an economic perspective, the cost of the device is considerable, but also towards the low side of the spectrum compared to other systems with the same functions. This is due to the full fabrication of the device with only the electronics components and the chemicals being bought externally. Further, the process of production is fully scalable, permitting a better transition towards a potential industrial future.

From an environmental perspective, the chemicals used are mostly organic compounds containing ethanol and silica which are unharmed to the environment and easily disposable. The process involves also low amounts of ammonia, which despite being toxic to the human health and the natural surroundings it's not enough to cause a significant damage. Even if the process was to be scaled, we made sure to use the fewest possible amounts without compromising the quality of the product.

1.4 Objective of the Thesis

The goal is to fabricate porous silica nanoparticles containing potassium (K^+) or oxygen (O_2) sensitive fluorophores for brain sensing. This encapsulation is anticipated to solve three issues: (1) restrict analysis to the extracellular space (2) lower the photobleaching rate of the fluorophores (3) allow co-localization of fluorophores with reporter fluorophores for quantitative ratio metric measurements.

Chapter 2

Background

2.1 Understanding the brain.

The brain is one of the most complex organs in our body that still requires plenty of research to be fully understood. It is responsible for controlling our behaviour, our body and who we are. As part of the nervous system (NS), the brain, along with the spinal cord are classified as Central Nervous System (CNS), while all the other peripheral bands of neurons classify as Peripheral Nervous System (PNS).

In the NS there are mostly two types of cells, the neurons and the glial cells. The first are used for the regulation and control of our whole body, the others instead fulfill multiple roles to assist, protect and maintain the neurons during their work [3].

2.1.1 The structure of the Neuron

The simple unit that composes the brain is the neuron. Neurons are some of the longest cells in our body as they can reach from brain to leg, such in the case for the sciatic neuron.

Generally, neurons can be divided into three parts as shown in Figure 2.1:

- The dendrites - responsible for receiving information from other neurons. On the dendrites specific receptors are present that inhibit or excite the cell when they bind with a specific ligand called neurotransmitters.
- The soma/cell body - main body of the cell, where the nucleus is.
- The axon - is a nerve fiber that unilaterally sends an output electrical signal called action potential (also called spike). At the end of the axon, there is an axon terminal that upon receiving the action potential releases quanta of neurotransmitter. Neuronal cells can only have one axon branch while having multiple dendrite branches.

The variations in the shape and structures of these three elements allows the presence of a vast array of different types of neurons, with different roles. These can be generalized

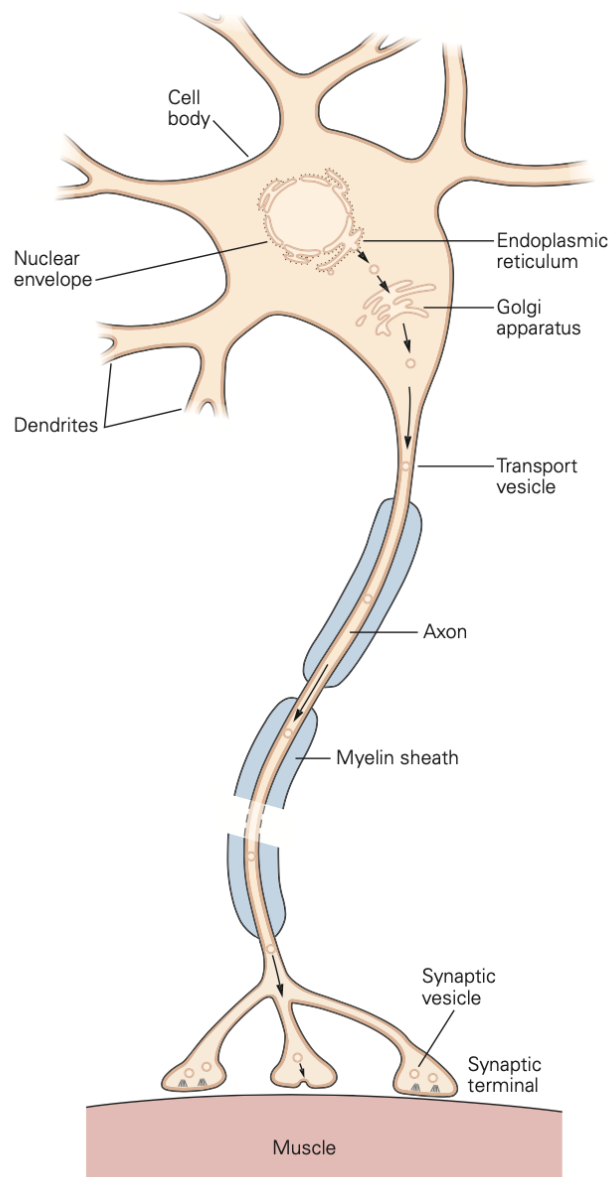


Figure 2.1: **The structure of the neuron.** The neuron can be divided in 3 parts: 1) soma or cell body containing the nucleus, this central area plays a crucial role in regulating the metabolic activity of the cell, protecting the genetic data and integrating the signal coming from the dendrites 2) dendrites which are branches extending from the soma and receiving information from other neurons or organs and passing it to the cell body 3) axon, which is the output branch coming out from the soma, often covered in myelin sheets to increment the speed of the signal and ending with synaptic terminals where through chemical or electrical signal it passes the information down to target organs or neurons. Adapted from [3].

in:

- Excitatory - Also known as pyramidal. These type of neurons cause a depolarizing effect on the dendrites they are projecting onto, making the postsynaptic neuron more likely to fire. These can further be subdivided into:
 - Local - These neurons present in layers 2/3 of the cortex are connected among each other creating localized smaller circuits.
 - Distal - These neurons are instead present mostly in cortical layers 4 and 5 and are characterized by their long axons that travel to distant brain regions.
- Inhibitory - Inhibitory neurons cause instead an hyperpolarization in the postsynaptic neuron, making it more difficult for it to fire.

Both types of Neurons are the main building blocks for our brain logic, allowing us to be capable of decision making. One of the ideal uses of our device would be to detect changes in the activity of all these types of neurons by monitoring in real time the changes in ionic concentrations.

2.1.2 The Action potential

To communicate and perform their functions, neurons use action potentials (AP). An action potential is a rapid change in membrane voltage (typically ranging from -70 mV to $+40$ mV on average) that travels down from the axon hillock (at the base of the soma) where it is generated and triggers the release of Neurotransmitter from the terminal into the neuronal synapses [3]. Depending on the receptors at the synapses, the neurotransmitter will have different effects.

The AP is triggered based on the received information from the dendrites which can either excite (increase the voltage) or inhibit (decrease the voltage) the neuron, with variation in intensity due to firing rate and number of stimuli. Further, for an AP to start, the sum of the received excitation and inhibition signals needs to overcome a certain threshold voltage (generally -55 mV), if this value is not reached, the AP will not start.

2.1.3 The chemistry behind an action potential.

When discussing the action potential at a chemical level it is important to consider that the action potential is a brief change in charge in a nanometric region of the membrane of the axon (which is generally in the tenth of microns in diameter). Thus the chemical changes are minimal and do not affect the full axon at once.

The axon's membrane has always a resting potential which is due to an imbalance in ions between the intracellular matrix (ICM) and the extracellular matrix (ECM). The inside of the axon is rich in potassium ions (K^+) and negatively charged proteins

the outside instead contains large amounts of sodium (Na^+) and chlorine (Cl^-) ions dissolved in water.

The concentration gradient is then pushing K^+ towards the outside and the Na^+ towards the inside, while the electrostatic pressure pushes both ions towards the inside of the neuron. The membrane can then be modelled as a capacitor through the Hodgkin-Huxley Model, holding an electrostatic resting potential described generally by Nernst equation:

$$E_x = \frac{RT}{zF} \cdot \ln\left(\frac{[X_{out}]}{[X_{in}]}\right)$$

where E_x is the Potential of an ion x , R is the gas constant, T is the temperature in K° , z is the ionic valence, F is Faraday's constant and $[X_{out}]$ and $[X_{in}]$ are the extra and intracellular concentrations of ion x .

When the AP begins, the Na^+ selective channels, initially in resting state (closed) are the first to open entering in an activated state. This causes inward current of positive ions and a depolarization which starts to spread down the axon due to the concentration gradient. These ion selective channels enter then in an inactivated state where they are still open but change conformation, blocking the flow of ions. This has the advantage of preventing the action potential from spreading backwards as well as being the main reason for a refractory period in which the action potential can't fire.

The K^+ channels open right after the Na^+ channels close, releasing the positive K^+ ions outside, in an outward current and causing the repolarization where the voltage goes back being negative.

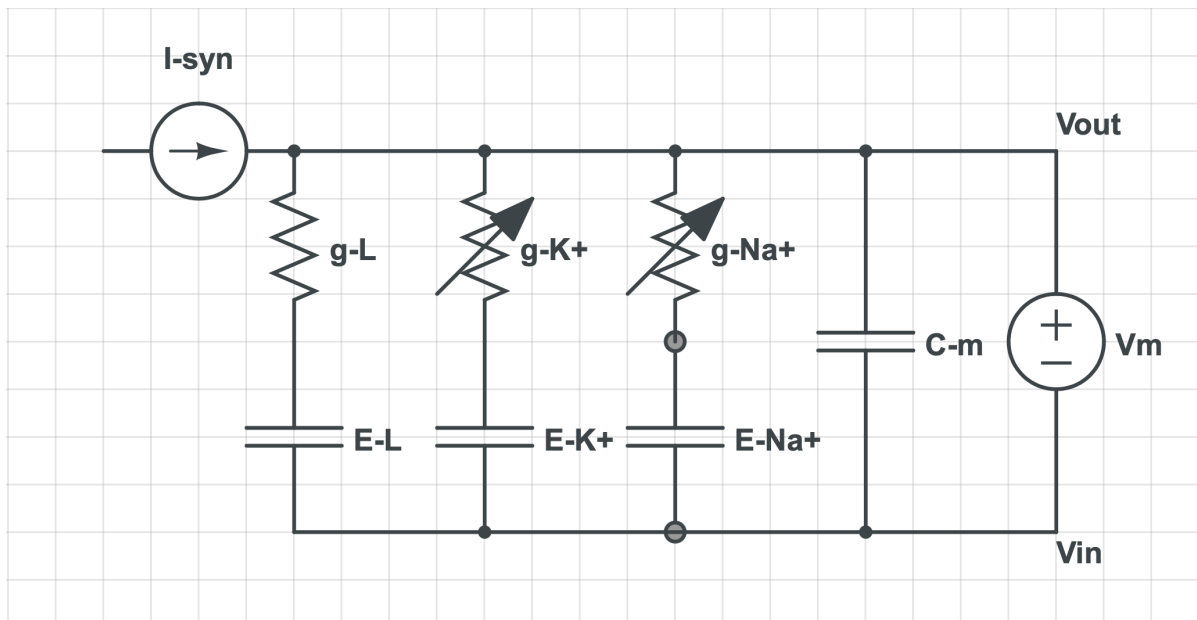


Figure 2.2: The axon's membrane modelled as an electrical circuit.

Considering the voltage gated channels as resistors in series with a capacitor as shown in figure 2.2, the total membrane current is then defined as the sum of the following currents:

$$I_{syn} = I_L + I_{K^+} + I_{Na^+} + I_{C_m}$$

Where I_{syn} is the synaptic input, I_L is the leakage current, I_{K^+} is the current through the Voltage Gated (VG) potassium channels, I_{Na^+} is the current through the VG sodium channels and I_{C_m} is the capacitance of the membrane itself. Both Na^+ and K^+ currents can be modelled using Nernst equation:

$$I_{K^+} = \bar{g}_{K^+} n^4 (V_m - E_{K^+}) = \bar{g}_{K^+} n^4 (V_m - \frac{RT}{zF} \cdot \ln(\frac{[K^+]_{out}}{[K^+]_{in}}))$$

where n is the probability that a sub-unit of the VG K^+ channel is in the open configuration, \bar{g}_{K^+} is the maximal conductance of the VG K^+ channels and the V_m is the membrane voltage.

$$I_{Na^+} = \bar{g}_{Na^+} m^3 h (V_m - E_{Na^+}) = \bar{g}_{Na^+} m^3 h (V_m - \frac{RT}{zF} \cdot \ln(\frac{[Na^+]_{out}}{[Na^+]_{in}}))$$

where m is the probability that a sub-unit of the VG Na^+ channel is in the open configuration while h is the inactivation constant which gives the probability that the channel is in the inactive state. \bar{g}_{Na^+} is the maximal conductance of the VG Na^+ channels.

At this point, the ions are in opposed positions compared to where they were initially. The high concentration of intracellular K^+ is then the main element in forming the difference in electrical and chemical gradient. In the meantime the Na^+/K^+ pumps slowly pump out 3 Na^+ ions and pump in 2 K^+ ion consuming Adenosine TriPhosphate (ATP) in the process [3]. All this mechanism results in a change in the potential and conductance of the Na^+ and K^+ channels as well as of the axon as shown in figure 2.3.

2.1.4 Studying the brain.

In the adult brain there are about 86 billion neurons. It might now be clear where the complexity in understanding and modeling the functioning of the millions of neuronal circuits and the necessity for tools to analyze them.

The methods and techniques to study the brain are many and divide the experiments in two different types:

- In Vitro experiments - These are tests that are performed on cells and tissues that are grown or have been removed from organs.
- In Vivo experiments - These are tests that are performed on living subjects, generally animals.

While in vitro experiments are generally a good way to study phenomenons in the brain isolating them it is important to also be able to replicate, when possible, in vivo, to observe the effects of the study on the full system and have a full understanding of the function of each component.

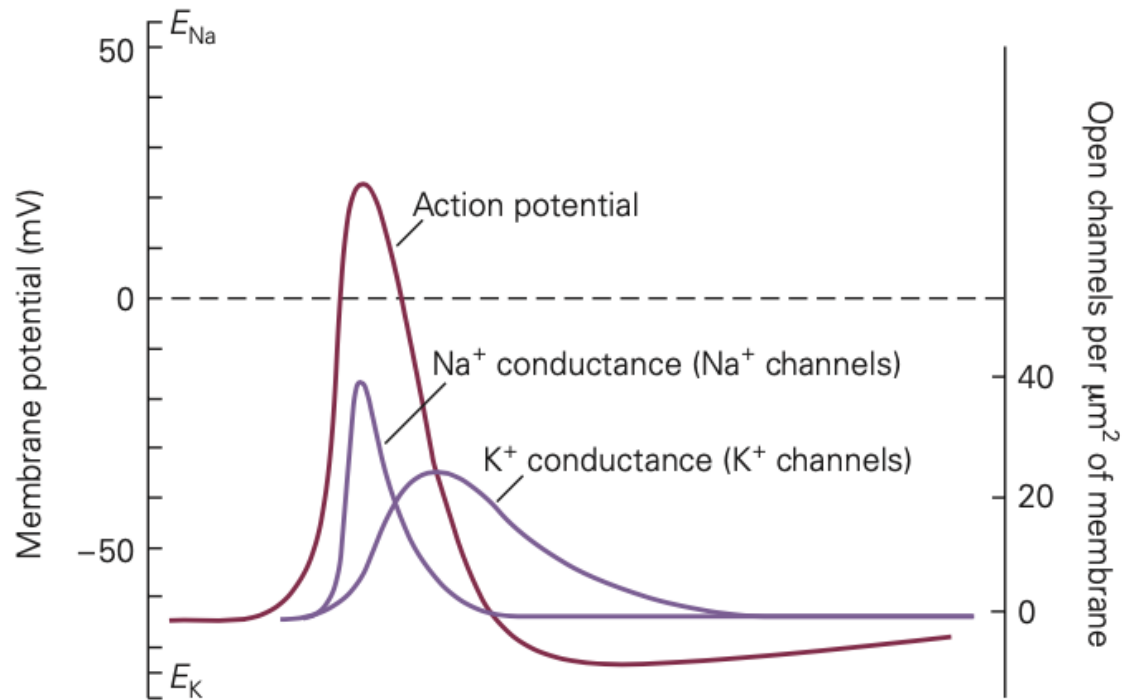


Figure 2.3: **The action potential and sequential conductance of voltage gated Na^+ and K^+ channels.** Adapted from [3].

2.2 Epilepsy

Epilepsy is a chronic disease that consists in the presence of seizures: waves of abnormal electrical activity in the brain affecting behavior and bodily control, often resulting in serious damage to the person if not helped. [4] There is currently no cure to Epilepsy, however with anti-seizure medications it is possible to reduce the severity and number of events experienced.

Unfortunately, there are downsides to this type of medications. First of all they are fully effective only on 66% of the patients. Second, these drugs have severe side effects, ranging from drowsiness, body problems but also cognitive and speech issues.[5] Common causes of epilepsy are injury from concussion, infection or even tumor. Other common major factors that increase the risk of epilepsy have been tracked to be genetics, strokes or birth complications. This makes of Epilepsy a complicated problem that is in need of new tools to be studied and solved.

2.2.1 Spreading Depolarization

Spreading Depression (SD) was first discovered and recorded in 1944 from Leão [6] as an abnormal suppression of the neuronal firing right after a seizure in the area of the cortex

of a rabbit (Figure 2.4). This silencing was named "spreading depolarization" because of its depolarizing effect on the cells which would prevent them from firing. It was later discovered at the end of the 1940s that the propagation speed of this phenomena was the same of migraine aura and was confirmed in recordings of migraine aura in patients.

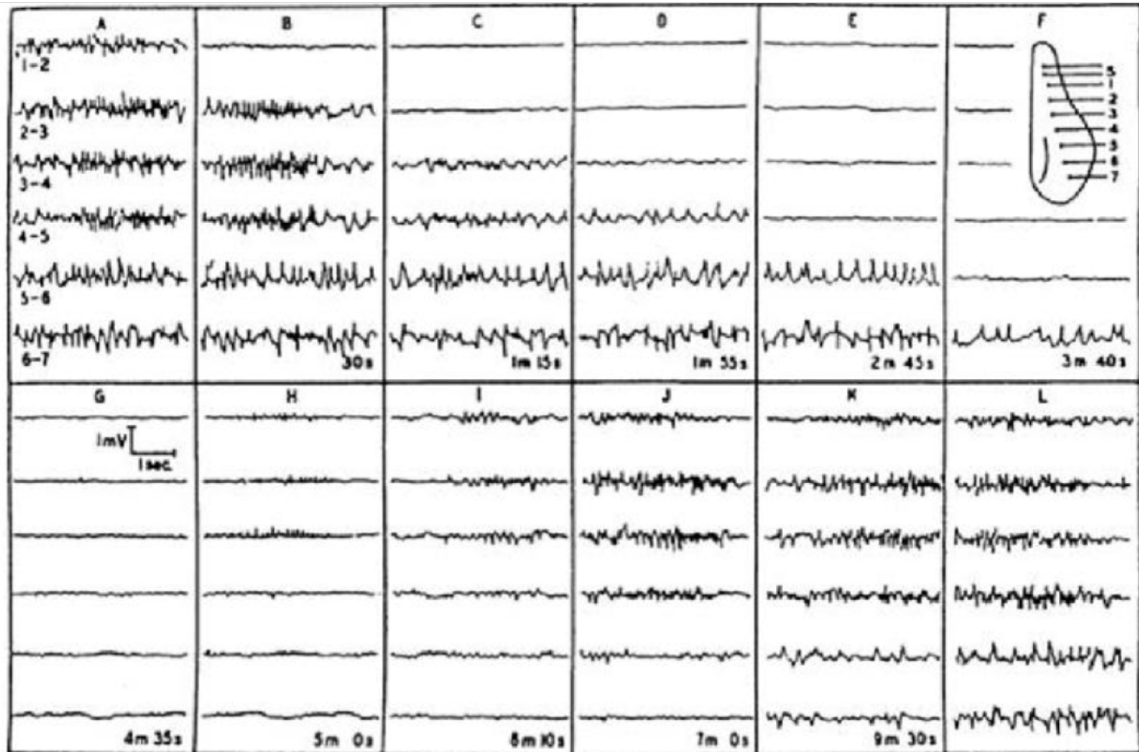


Figure 2.4: **First evidence of Spreading depression.** Adapted from [6].

At the end of the 1980s, thanks to chronic neuronal intracellular studies, SD gained increasing attention in the Epilepsy community since it might be related to Sudden Unexpected Death in Epilepsy (SUDEP), postictal amnesia, and postictal generalized EEG suppression (PGES) [7].

SD is a slow propagating wave of neuronal depolarization causing major abnormalities in ionic cellular concentrations, deriving in silencing of the electrophysiological activity across large cortical regions in the brain. It is understood that SD generates a shift in extracellular potential up to 30 mV with frequencies below 0.01 Hz, imposing a challenge for traditional high pass amplifiers used in EEG. The major area targeted by this effect is sector CA1 in the hippocampus, making it one of the most common dissected areas for the study of the disease [8].

2.2.2 Measure Analyte concentrations in the brain

Hypoxia is a condition consisting in the lack of sufficient oxygen in the tissue. Oxygen is a key element in the mitochondrial respiration in the cells, since it permits the formation of ATP through the process of oxidative phosphorylation. ATP is the main source of energy in the body, particularly in the brain where its presence is required constantly to activate the ionic pumps. This means that when no oxygen is present, no ATP is produced and the pumps as well as other elements of the neurons stop working, making the cell die through apoptosis. This associates the lack of oxygen to diseases such as anemia, cardiac complications, cancer and stroke.

A tool designed to constantly measure the oxygenation of the tissue in the brain would then be important to quantify the health of the organ, observing its metabolism and regulation of the oxygen parameter [8]. Further, a way to measure O_2 concentration with high spatial and temporal resolution would also allow a better insight in diseases that affect this parameter such as epilepsy, Alzheimer's or Huntington's.

O_2 sensors development has been a topic of high interest in the past 10 years. Despite the presence of indirect techniques (such as hemodynamics or metabolic change analysis) and direct techniques (such as electron paramagnetic resonance), which have been used in the past, there is still a lack of high resolution in the spatio-temporal domain.

It has been mentioned already that during SD there is an ionic imbalance that causes the neurons to swell. One of the key elements causing this effect is an increase in the Extracellular matrix (ECM) of K^+ ions.

This increase in extracellular concentration of Potassium doesn't create enough current through the channel to hyperpolarize the cell, keeping it in a depolarized state, slowing the closure of the K^+ VG channels and increasing the concentration of ECM K^+ . This makes the action potential hit a quasi-steady state a few mV below its peak. It is then only up to the Na^+/K^+ pumps to bring the neuron back to resting potential, taking much more time than normal. In this period the neuron cannot compute as it is currently in refractory period.

Further, a higher concentration in the ECM of potassium might also raise the resting potential of the neuron, requiring a stronger depolarization for the neuron to fire and might even lead to the death of the neuron if the pumps are not able to function due to hypoxia.

Finally, the high concentration of K^+ ions in the extracellular matrix will spread through diffusion. The brain has a high density of neurons meaning that the ECM is very small, meaning that the high concentration of potassium might (and usually does) reach nearby neurons which are then similarly affected. This would then be explaining the propagation of the depolarization that is observed in SD as well as the silencing. All these effects were simulated using the Hodgkin-Huxley model [9] represented in figure 2.5 and show the behaviours expected and described before

Current common techniques use staining and K^+ sensitive microelectrode record-

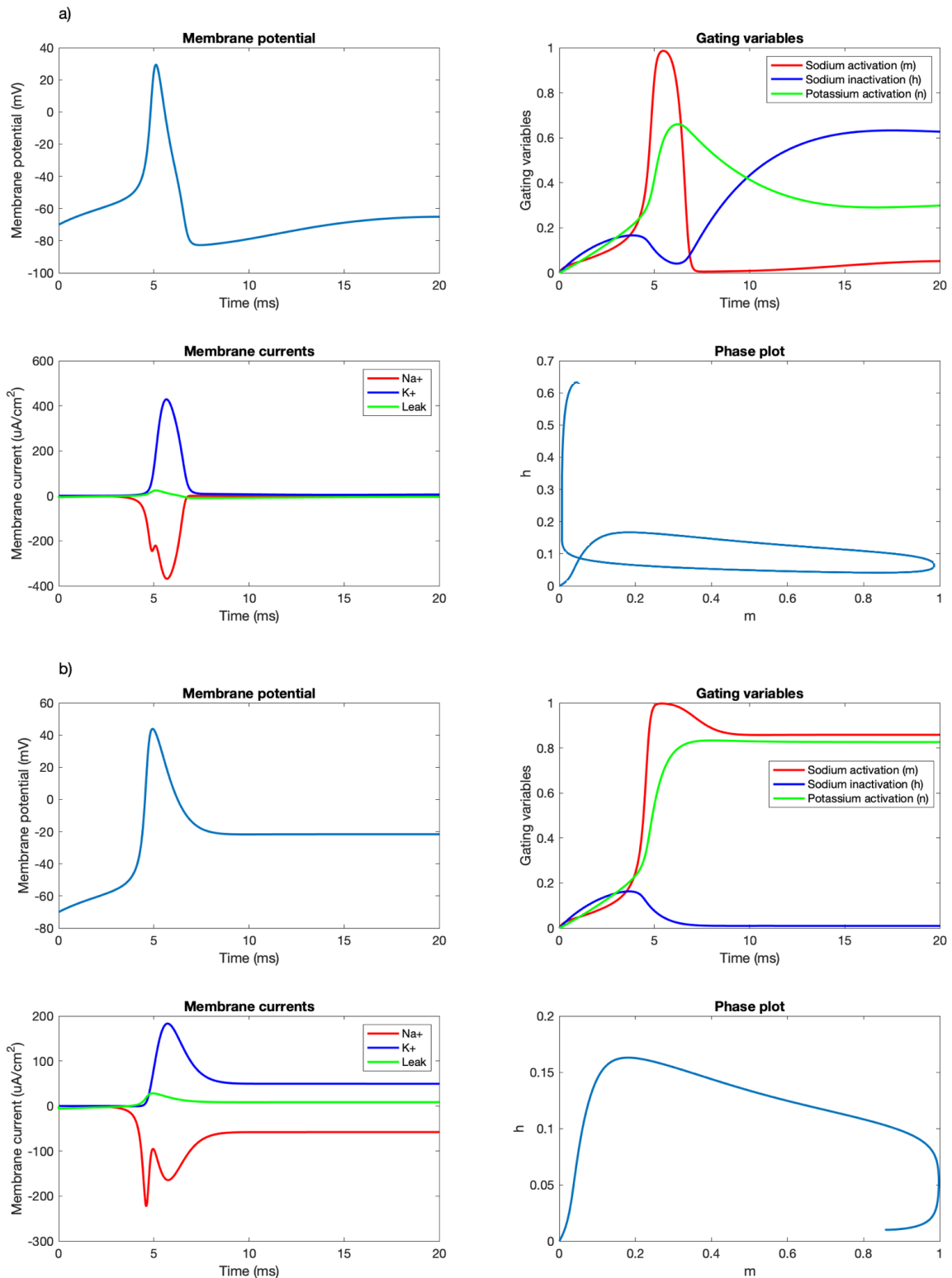


Figure 2.5: **Effects of Spreading Depolarization on the Action Potential.** a) Action Potential as a function of time, ionic currents and gating variables in a neuron with normal ionic balances. b) Action Potential as a function of time, ionic currents and gating variables in a neuron with high levels of extracellular potassium (condition observed generally during SD).

ings, however both techniques lack, similarly to oxygen recordings, high spatial and/or temporal resolution, indicating the need for a tool to be able to monitor and map the rapid changes of these analytes in in-vivo experiments [10].

2.2.3 Optical probes for Concentration sensing

Fluorophores have been engineered in the past 20 years to be used in biological studies by making them bio-compatible and alter their luminescence based on the binding with specific analytes.

When a fluorophore is excited the energy absorbed changes temporarily the chemical structure of the molecule (for example shifting the configuration from *-cis* to *-trans*), in doing so, the energy absorbed decreases and as the structure goes back to the initial shape it will emit the remaining energy in the form of light with a different wavelength from the absorbed one. If the fluorophore is sensitive to a specific analyte, this shift in chemical structure happens only when the analyte is bound to the substrate. If not bound no excitation and consequently no emission will happen.

There are multiple available options for K^+ and O_2 sensitive fluorescent probes, however a recurring problem in most of them is their tendency to photobleach or photobleaching rate.

Photobleaching happens when too much energy is absorbed causing a full permanent shift in the chemical configuration, often breaking the molecule, providing a significant limitation of this techniques. This means also that in the long term, the concentration of functional fluorophore decreases, making long term in vivo quantitative imaging difficult [8] [11]. Despite photobleaching, these analyte sensitive fluorophores can then be used coupled with a reference dye to measure ratiometrically, the concentration of either O_2 or K^+ , modelling the intensity of light following the Stern-Volmer trend and the amount of fluorophore necessary based on the Beer-Lambert law [10].

A key advantage of using fluorescence imaging for ion concentration quantization is to use FRET excitation. Fluorescence resonance energy transfer (FRET) is a cascade process through which energy is transmitted non-radiatively from a donor fluorophore to an acceptor fluorophore, allowing the latter to express its fluorescence. This is a distance dependent characteristic that can only happen within 10 nm range from the donor and that can be used to excite other fluorophores in multiple emission ranges.

2.2.4 Motivation

In 2022, Gangarosa [2], presented an Oxygen Sensing measuring system that made use of fiber optics to measure oxygen concentration using different O_2 sensitive fluorophores and quantum dots. Her system worked but lacked calibration and alignment of the photodiodes due to the setbacks imposed by the quantum dots applications.

What we are suggesting is a sensor that can be directly bound to the surface of an optic fiber probe and interface with Gangarosa's optic endoscope [2]. To build it we are using engineered Silica Porous Nanoparticles containing analyte specific fluorophores for ratiometric analysis.

Through the encapsulation, the fluorophores would be partially restrained which would result in a lower emission but that would also prevent photobleaching. Further, the use of these nanoparticles would allow customization of the analytes to monitor as well as the FRET excitation cascade and the ability of measuring the concentration of multiple parameters at the same time, limiting the recording area to only the ECM for extended periods of time.

This will permit quantitative in vivo studies of oxygen and potassium concentrations during SD and their changes when passing from healthy to diseased state or during a seizure[11]. Further, this technology will be able to be translated to other studies due to the configurability of the system and the versatility of the sensor.

Chapter 3

Previous systems

3.1 An Optical Endoscope for analyte sensing

In 2022, Gangarosa built a device that using light could ratiometrically determine the fluorescence of a dye with the intention on using it to determine the local concentration of specific analytes in brain in vivo experiments [2].

In her tests she used quantum dots to test the optic endoscope, however these dyes are not feasible for in vivo application due to their toxicity and rapid degradation. Thus, for this reason there is the need for a biosafe sensor that can be applied on the system, emit a reference signal and at least a modulated signal that varies its intensity proportionally and specifically to a single analyte.

The system of the optical endoscope is illustrated in figure 3.1 and its functioning can be summarized in the following steps:

1. **LED light source** - An external LED driver determines the intensity of the LED chosen of a wavelength that will be able to excite the fluorophore. The light is sent inside of an optic fiber cable to the next component of the system.
2. **90:10 Coupler** - The light from the LED enters in the coupler from the port 1 and is separated according to the ratio indicated: approximately 90% of the signal is passed through at port 4, while the remaining 10% is sent to port 3 (where the probe is) and it is reflected back. This is because reflecting too much light can interfere with the initial system creating unreliable analysis. It would be convenient considering for power optimization the use of an optical fiber circulator which fully reflects the signal entering in port 3 without loss.
3. **Probe** - The light entering the probe is passed through a coating at the tip of the fiber, which is injected in the area to monitor either in vivo or in vitro. Based on the environment, the light is modulated and proportionally to the concentration of analyte of interest, emitted back through fluorescence by the coating, along with a reference fluorescence signal. This coating is the sensor that in Gangarosa's paper was made of Quantum Dots, but that will be replaced by the sensor produced in this paper.

4. **Light collimator** - The light entering the coupler is splitted again in proportion, meaning that 10% of it will pass to port 1 while 90% of it will be passed through port 2. Respectively we would expect port 1 and 2 to receive 1% and 9% of the input intensity. The light entering port 2 will then be emitted as a parallel beam thanks to the collimator towards the dichroic mirror in a darkroom.
5. **Dichroic mirror and photodiodes** - The dichroic mirror separates the received light beam based on whether the wavelength is above or below a certain threshold (the emission wavelength of the analyte sensitive fluorophores in our case). The two beams are then detected by two photodiodes that record the intensity of each signal sending the information to the computer which in this way can ratiometrically determine the concentration of the analyte in real time with high spatial and temporal accuracy.

3.2 Nanoparticles as analyte sensors

Before designing our own sensor for light modulation on the endoscope, we looked into past important achievements in the field of nanoparticles for biomedical application. We observed the methods of synthesis, the tests and balanced the advantages and disadvantages, to understand how such technologies can be made, analyzed and applied for our purpose.

3.2.1 C-Dots: fluorescent biomarkers Core-shell silica nanoparticles

Cornell Dots or C-Dots are a new innovative type of Quantum dot with a radii between 10 and 15 nm first presented by Wiesner in 2007 [12]. Under excitation each C-dot can emit more than 10 photons in the time a fluorophore emits 1. This, the lack of toxicity due to the use of Silica and the small size makes it an ideal tool for in-vivo, size selective analysis. However they require an expensive process to be produced and their stability varies over time, resulting in a decrease in fluorescence. The advantage of CDOTs is that they can be tuned at different emission wavelengths with great photostability and bioluminescence.

Due to the great advantages that this tool has, CDOTs have been slowly started transitioning to clinical trials and currently passed the FDA criterias [13], opening the way for future similar products such as ours.

Synthesis of C dots (30 nm diameter) was made by conjugating OG488 (also known as TRITC) through isothiocyanate group to APTS at a ratio of 1:50 in absolute ethanol and diluting the result. To this a silica precursor (Tetraethyl orthosilicate or TEOS) was added at 0.05 M. The result was left resting for 8 h, after which more TEOS was added in intervals of 15 minutes. The particles were left reacting for other 24 h and

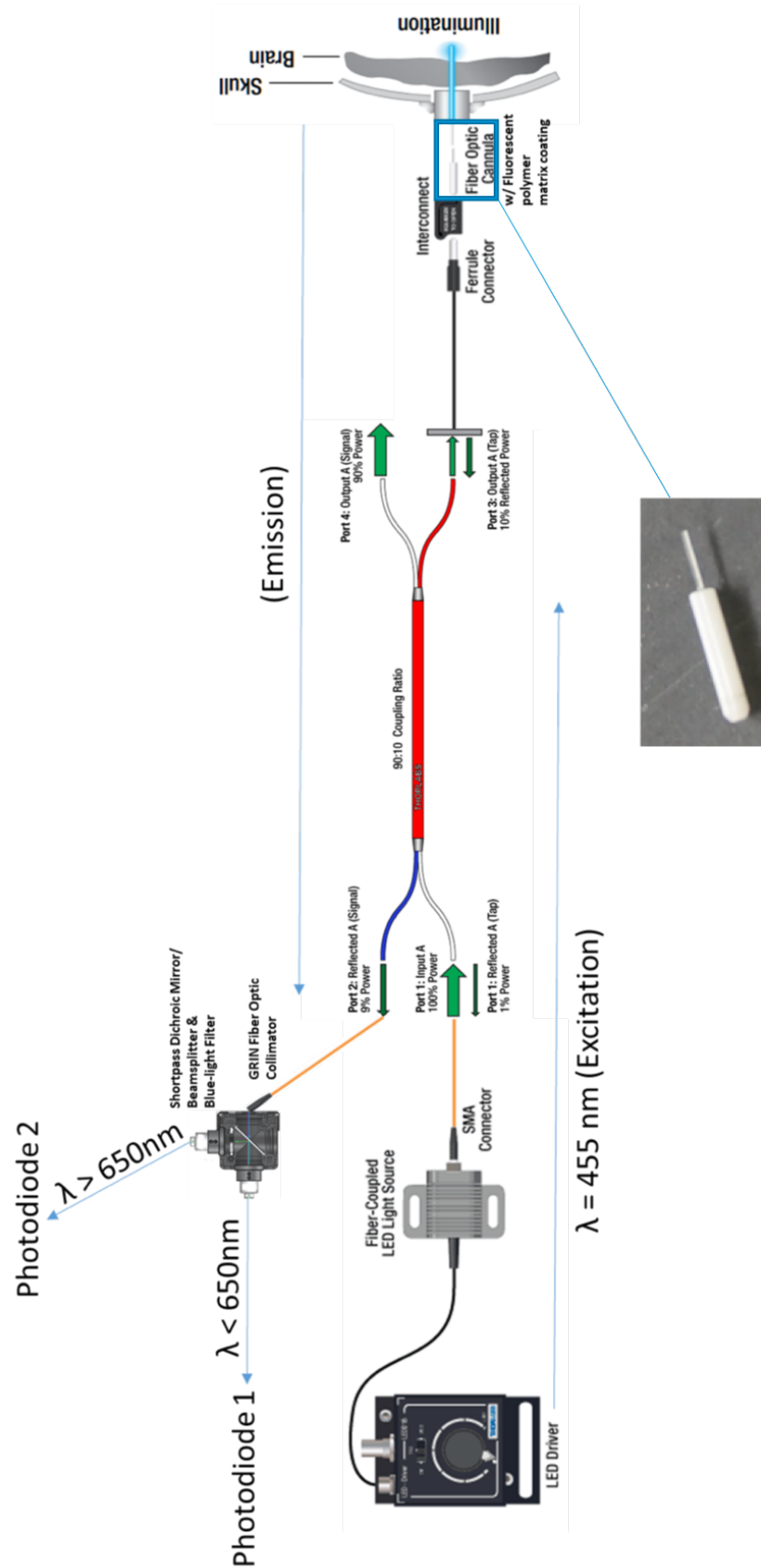


Figure 3.1: Optic endoscope for localized analyte monitoring system breakdown. Adapted from [2].

then dialyzes.

Toxicity Experiments were performed by injecting different concentrations of C dots in the tail vein of mice and progresses were recorded over different times (1, 3, 7, 21 and 60 days). The animals were observed daily. As a result, no abnormal clinical sign was noticed, even at the highest concentration tested ($0.33 \mu\text{M}$).

Distribution evaluation was performed by staining (using DAPI) and using a custom image analysis software. The distribution analysis revealed high presence of C dots in particular in cells of mono nuclear phagocyte system (Kupffer). Further, at $0.33 \mu\text{M}$ the C dots in the liver were consumed by macrophages in months (losing a fluorescence at a rate of about 25% per month).

Lymph Node mapping was done using C dots to test their efficacy. The tuning of the surface of the C dots. It worked but they had to use a stain to highlight the difference in cell. Injection of multiple C dots with different colors was excellent to highlight different cell types.

3.2.2 Multiplex analysis probes

Synthesis of Nanoparticles (70 nm diameter) was made through two steps microemulsion of RuBpy doped porous silica core and Pas-DTPA silica shell. The shell had a shell thick 11 nm on average while the core was around 50 nm diameter. Both DTPA and RuBpy are dyes and emit in different spectra, probably this is why the NP are so big.

Ion binding tests were performed using the nanoparticles as probes with Tb^{3+} and Gd^{3+} . Both ions, indeed can bind with DTPA and emit different spectra of fluorescence. In this way, through the peaks it was possible to monitor concentration of both ions with the same probe, using RuBpy as control [14].

3.2.3 PSNP - Polystyrene nanoparticles for oxygen sensing

Synthesis of Nanoparticles (40-60 nm) The Polystyrene nanoparticles were produced using emulsion polymerization in the synthesis and the dye is then added as a mixture with 18C6 and THF [15]. This allows a wide range of applications depending on the coating that is being applied.

Oxygen sensing was an example of application of PSNPs, where they coated the particles with $[\text{Ru}(\text{dpp})_3](\text{TMSPS})_2$. Fluorescence testing in vitro showed a linear relationship between the concentration of oxygen and the fluorescence of the RuPSNPs with low levels of cytotoxicity [16].

3.2.4 PEBBLE nanoparticles - photonic explorer for bioanalysis with biologically localized embedding

Synthesis of Nanoparticles (20 nm) Acrylamide PEBBLEs produced by Kopelman for the first time in 1997 were formed through polymerisation solution and stirred under nitrogen while cooling. Other variants of this procedure are present using other polymers, depending on the function of the nanoparticle.

Applications These particles were produced with multiple applications, mostly in monitoring environment through the use of embedded fluorophores sensitive to O_2 and pH. Alternatives to fluorophores were peptides and proteins with a dye label attached to them that would emit light upon binding to specific molecules (NO)[17] [18].

3.2.5 CPNP - Calcium Phosphate Composite Nanoparticles

Synthesis of Nanoparticles (20-30 nm) The synthesis involves the self-formation of reverse micelles using two microemulsions. To one of these, depending on the properties, is added the dye or drug to be encapsulated and a third emulsion is used as dispersant. The reverse micelles dissolve through change in pH and they are then washed and ready for application [19].

Fluorescence Correlation was tested to measure the radii of the particles compared to the TEM data to confirm their morphology and colloidal stability.

Dissolution of the particles was tested at low pH, showing that the particles can be used to deliver drugs and fluorescent probes to target specific areas. Further confirmation was obtained through staining of bovine aorta.

Chapter 4

Selection of the dyes

To transduce the quantity of analyte in the analyzed area into a readable optical signal that can be understood from the system designed by Gangarosa [2], we decided to use fluorophores. A fluorophore is a molecule that emits light once excited at a certain absorption wavelength. The process of emission happens when the fluorophore absorbs energy in the form of light and enters in an excited state. Compared to the Quantum Dots and sensing dyes used in her thesis, the advantages of fluorophores is that they are biocompatible for the most part, allowing a safe use in biological environmental with minimal levels of toxicity.

The molecule stays in this state for an amount of time called **luminescence decay time**, when this is for long periods of time, the effect is not called anymore fluorescence but phosphorescence. Once the molecule stops being in its excited state, the energy is released in the form of light at a different wavelength.

Fluorophores that are sensitive to other analytes have generally a binding site to which the molecule can connect, which alters the fluorescence emission in different ways depending on the fluorophore:

- Intensity - The binding of the molecule quenches or increases the intensity of the emitted light
- Decay time - Once bound, the molecule can reduce or increase the luminescence decay time. This type of analyte-sensitive fluorophores are not commonly used since very precise and expensive equipment is required to measure the change in absorption and emission times.
- Spectra - Perhaps the most common type of light modulation for analyte sensing as well as the easiest to detect. When the binding site is occupied, there is a wavelength shift in emitted light from the fluorophore.

For these reasons, fluorophores are an excellent tool to monitor quantitatively the concentration of analytes or other factors such as pH or temperature. Their ability to modulate light based on whether the binding site is connected or not has been engineered enormously in the past years producing light sensors translatable to any application [20] [21].

4.1 Criteria

When choosing a fluorophore for biomedical application to measure certain values (such as ionic concentration, pH or temperature) it is important to consider several factors that might impact the decision of the probe [22] [23] [24]:

- **Absorption and Emission spectra** - UV excitation should be avoided, as it can lead to background fluorescence and interfere with certain systems. Instead, red or near-infrared (NIR) excitation is typically preferred for tissue monitoring, as these wavelengths have less background fluorescence. Additionally, large **Stokes shifts** (the distance between absorption and emission peak) are desirable, as they make optical filtering easier.
- **Intensity** - the brightness of the probe depends on the formula

$$I = \varepsilon \cdot \Phi$$

where ε is the molar absorption coefficient, or the amount of light at a certain wavelength that the fluorophore can absorb, and Φ is the luminescence quantum yield, or the efficiency with which the fluorophore converts absorbed light into emitted one.

It is generally good for a probe to have a high brightness since that means that less indicator needs to be used.

- **Luminescence decay time** - Depending on the application of the sensor, longer times might be preferred for easier time analysis, however shorter times are more favorable for more dynamic sensors.
- **Cross sensitivity** - The fluorophore needs to be able to modulate light only based on the interaction with only one factor in its environment and not multiple. A common effect to be aware of is the thermal quenching which happens in certain molecules above a certain temperature, causing a decrease in efficiency of the light emitted. It is thus important to limit cross sensitivity to minimum, to prevent inaccurate readings.
- **Photostability** - Fluorophores to emit light undergo an excited state during which there is a chance of the molecule breaking due to alteration of its chemical structure depending on the intensity and duration of the absorbed light, this is called **photobleaching**. The photostability of the molecule is its ability of maintaining its properties and not photobleach. Having good photostability is an important factor for situation where the fluorophore is exposed for extended amounts of time to light or in harsh environments.
- **Solubility in the media** - The solubility of the nanoparticle construct in the media (such as 70/30 Ethanol/Water aqueous solution) is key for it to not create

aggregates. The latter can alter the analysis of the data causing incorrect results. It is possible to use polar groups to anchor to either the fluorophores or nanoparticles or to increase the either parts' solubility.

- **Toxicity** - the fluorophore should be non toxic and bio compatible, to prevent intoxication of the tissue as well as of animal test subjects. In case toxic fluorophores need to be used, encapsulation of the molecules and lower concentrations of it can be used as mitigating solutions to prevent adverse effects.
- **Availability** - Finally, it is important to consider how complicated it is to obtain the fluorophore of interest. Most common fluorophores are commercially available, however more sophisticated ones can be difficult to be bought premade as they require particular synthesis procedures and might require the researchers months and expensive resources to get accustomed to the synthesis and produce reliable fluorophores.

4.2 A review of O_2 sensitive fluorophores

Oxygen is one of the major analytes along with potassium that is targeted by many diseases such as epilepsy and spreading depression. Indeed, it has been noticed that during spreading depression there is a sudden decrease in O_2 concentration in the area that is being affected.

Due to this necessity and interest in monitoring Oxygen levels locally, we looked into possible probes sensitive to this analyte to encapsulate. Since the early 2000 there has been an in depth research and development for commercially available sensors for oxygen monitoring for multiple application. The main categories of dye are being summarized in table 4.1.

Fluorophore Class	Advantages	Disadvantages
Reversible Probes	<ul style="list-style-type: none"> • Mimic the structure of hemoglobin 	<ul style="list-style-type: none"> • Low Resolution • pH dependent

Polycyclic aromatic hydrocarbons (PAHs)	<ul style="list-style-type: none"> • Long time luminescence • High quantum yield • Longer fluorescence lifetime • Rapid response and recovery times • Absorption maximum coincides with second harmonic emission of near IR from semiconductor • Can be excited by blue LED • Doesn't produce singlet oxygen when quenched 	<ul style="list-style-type: none"> • Short excitation wavelength which results in a strong background fluorescence • Low molar absorption coefficient resulting in moderate brightness • Fluorescence decay times are lower than several hundred nanoseconds, limiting sensitivity in less permeable matrices • Lack of stability, tending to diffuse out of the support or evaporate, and aggregate in polymeric matrices.
Transition metals polypyridyl complexes	<ul style="list-style-type: none"> • Possess excitation and emission maxima in the visible region • Show good photostability • Luminescent properties can be tuned as a function of the ligands 	<ul style="list-style-type: none"> • The resolution of such sensors in the range is often not sufficient for practical applications
Metalloporphyrin	<ul style="list-style-type: none"> • Moderate to high molar absorption coefficients • Large Stokes shifts • Good brightness when excited in the Soret band (350 to 450 nm) 	<ul style="list-style-type: none"> • Excitation in the Q band (500 to 700 nm) does not produce efficient brightness.

Cyclometallated complexes	<ul style="list-style-type: none"> • High molar absorption coefficients • Large Stokes shifts • Strong Photostability 	<ul style="list-style-type: none"> • Decay time in the ms range (which might cause background fluorescence) • Difficult to obtain
---------------------------	--	---

Table 4.1: Advantages and disadvantages of the main fluorophore groups for Oxygen Sensing. The data extracted from [22] [24].

Thus, after reviewing the different types of Oxygen sensitive dyes, we identifies the following fluorophores as candidates for oxygen measurements to be considered to be encapsulated:

- *Pt(II) porphyrins* from the Metalloporphyrin group - Aside from the general advantages described before, they have very high emission, equivalent to 2-3 times the one of other porphyrins, making them more effective for our use. Gangarosa in her paper [2] used indeed PtOEPK which is part of this group.
- *Pt(ddp)(CN)₂* from the Transition metals polypyridyl complexes group - Differently from other polypyridyl complexes, the ones using Pt(II) tend to not leach (fluorophore detaching from the carrier, in our case it reduces the leakage from the nanoparticle.) when exposed to aqueous solutions. Further, Pt(ddp)(CN)₂ forms excimer which emits light during decay making it easier to monitor the oxygen levels.
- *Cyclometallated Iridium(III)* from the Cyclometallated complexes - differently from other cyclometallated groups this one overcomes the low molar absorption and emits with strong phosphorescence. It is generally used to monitor fast processes, making it optimal for our application. Finally, its spectral properties can be regulated using coumarin substitutes.
- *Pt(thpy)₂* from the Cyclometallated complexes - Pt(thpy)₂ also shows high luminescence quantum yield and long lifetime. Also, it is non water soluble and not susceptible to leaching when in it.
- *ddpePtP2* from the Cyclometallated complexes - An interesting and useful characteristic is that this fluorophore has a dual emission, which can be used for ratio-metric measurements, removing the need for a reference dye.

4.3 A review of K^+ sensitive fluorophores

Potassium is also a key ion to be affected by many neuro-related diseases, since it is correlated to the action potential. During Spreading Depression indeed, the concentration of K^+ ions in the extracellular matrix increases abnormally, causing the bloating of the neuron and spreading to nearby cells, causing the wave of neuronal death.

Unlike with oxygen, not much research has been done on commercially available potassium sensitive fluorophores, and most of the ones that are available are often very sensitive to sodium and/or calcium ions too, thus not being suitable for brain applications. The potential candidates for monitoring this analyte were then few:

- *APG₄ (Asante Potassium Green 4)* - Also known as Ion Potassium Green 4 (IPG4), this seems to be the only commercially available K^+ fluorophore that is significantly more sensitive to K^+ than Na^+ and that could be applied for our sensor. However, the big disadvantage of the dye is that it has a very small Stokes shift (20 nm) making it very difficult to distinguish the peaks. [25]
- *PBFI (Pyridine-based potentiometric fluorescent indicator)* - PBFI has very large stokes shift (about 200 nm), however its excitation is in the UV range which can cause autofluorescence from the cells. Further, PBFI has also a minor but still relevant selectivity to Na^+ which differently from APG4 is not negligible.

4.4 FRET excitation for multiple analyte monitoring

Förster Resonance Energy Transfer also known as FRET excitation is a phenomena that was first discovered and described by Theodore Förster in 1948. This effect is a transferring of energy happening between two fluorophores, one excited called donor and one not excited called acceptor. When the the donor is in close proximity to the acceptor some of the donor's energy is passed onto the other molecule, causing the latter to excite [26].

In the specific, the donor fluorophore is absorbing energy corresponding to its absorption spectrum and it is emitting energy in its emission spectrum. If the emission spectrum of the donor partially overlaps with the absorption spectrum of the acceptor, a part of the emitted light from the donor will be absorbed by the acceptor. The extent of this absorption depends on the proximity of the two molecules, as shown in figure 4.1.

The efficiency for this transfer depends on multiple factors, including but not being limited to: the distance between the two fluorophores, the absorption and emission spectra of the donor and acceptor, the orientation of the molecules' dipoles and the medium through which the interaction takes place.

This property of fluorophores can be used for the formation of FRET couples within the nanoparticles and monitor contemporaneously multiple parameter as well as reducing the quantity of light sources needed for exciting the fluorophores. When choosing a FRET pair, it is important to consider the absorption/emission spectrum of the donor and acceptor fluorophores, so that the curves overlaps as much as possible. Next, it

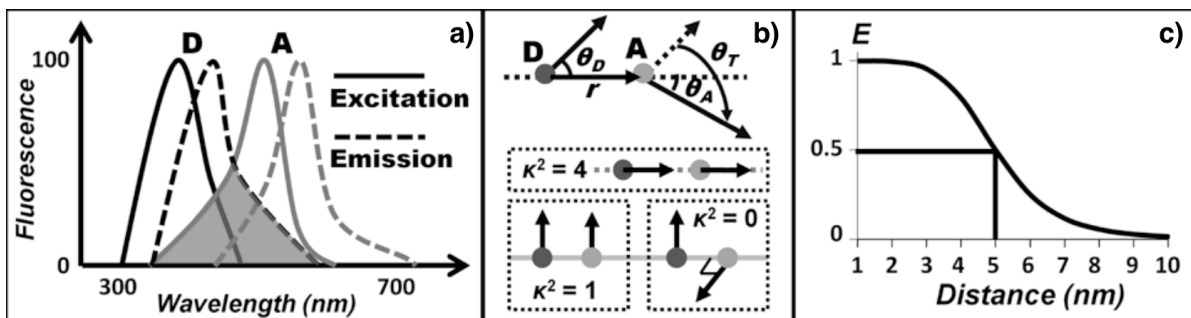


Figure 4.1: **Basic concepts for FRET excitation to be achieved [26]:** a) the emitted spectrum of the donor needs to be at least partially overlapping with the acceptor's absorption spectrum. b) the dipole moment κ^2 needs to be as large as possible to increase the chance of FRET and should not be 0. c) The efficiency decreases with the distance of the two molecules following a sigmoidal trend where the efficiency drops to 0 after a delimited R_0 or Förster distance, generally of 10nm.

is necessary to understand the density of donors and acceptors to estimate the average distance between each using the following derived formula:

$$d_{avg} = \sqrt[3]{\sum_{i=1}^n \frac{1}{N_A \cdot C_i}}$$

where N_A is Avogadro's number and C_i is the concentration of fluorophore i in the solution.

Chapter 5

Methods and Results

To monitor the concentrations of analytes in real time with high spatial and temporal resolution we need then to design and develop a sensor. This sensor needs to be able of monitoring multiple analytes at once by containing multiple fluorophores. The sensor needs also to be highly microporous (pore size $<2\text{nm}$), so that the dyes cannot leak out from it but the ions and small molecules can still enter, interacting with the fluorophores. Finally, the sensor needs to be strongly connectable to a fiber stub to make it interfascable with the light endoscope designed by Gangarosa [2].

To design the sensor we decided to start from a reliable procedure to synthesize biocompatible nanoparticles based of the one outlined from Werner Stöber [27]. We then proceeded by identifying a way to modify it to add porosity and control the size of the particles. Finally we encapsulated a fluorescein, a test fluorophore to understand how its properties are affected by the silica shell.

This chapter will first explain the chemistry behind the Stöber procedure and the motivations that led to this choice. The characterization methods will then be listed and explained to understand how the data was gathered, analyzed as well as listing some of the major limitations of each method. Finally, the chapter will present the methods explained in depth along with the results obtained and their interpretation.

5.1 The Stöber procedure

In 1968 Werner Stöber presented a new method in his paper "Controlled Growth of Monodisperse Silica Spheres in the Micron Size Range"[27] to produce silica nanoparticles. The procedure revolves around the hydrolysis of the orthosilicate *Tetraethylorthosilicate (TEOS)* in ethanol, water and ammonia. Through the concentration of the reagents it is possible to have full control over the size of the produced nanoparticles permitting a range between 50 nm and 1 μm [27]. This procedure offers several advantages:

- *Monodispersivity of the solution* - The polydispersivity index (PDI) of a solution

is a factor that indicates the variation in particle mass/size in a solution. The higher this value is, the wider the variation in particle size in the solution. A solution that is monodispersed means that the particles present in the solution are all approximately the same in size with very few variation. A solution is defined as monodispersed if its PDI is less than 0.1 and highly monodispersed if below 0.07 [28]. The Stöber procedure reliably produces monodispersed nanoparticles.

- *Scalability* - This procedure is fully scalable meaning that with the increment or decrease of the quantities, the reaction doesn't change and doesn't decrease in effectiveness even when replicated in large scale [27].
- *Ease* - The reaction is simple to perform not requiring advanced equipment or specific conditions, making it an economic method for production of nanoparticles.

Overall the Stöber procedure is highly reliable and that has been widely used for production of silica nanoparticles for multiple functions [29].

5.1.1 Reaction breakdown

The reaction used in the traditional procedure designed by Stöber in the late 60s can be divided in the following three steps [27][29][30]:

1. **Hydrolysis** - When TEOS is added to the solution of ethanol, water and ammonia, it hydrolyzes, meaning it reacts with the water, forming silanol groups (Si-OH). This reaction is catalyzed by the ammonia, which increases the pH of the solution.
2. **Nucleation** - The silanol groups react with either other TEOS molecules or SiOH groups passing to the solid phase and converting to siloxane (Si-O-Si) and creating what are called 'nuclei'.
3. **Growth** - Once the nuclei have been formed, the free silanol groups still left in the solution attach through aggregation to the nuclei making them grow and increasing their size. In this step ammonia acts as a stabilizer preventing the growth beyond a certain size following the chart in 5.1.

5.2 Characterization methods

5.2.1 Dynamic Light Scattering Analysis

Dynamic Light Scattering, also known as DLS, is a method to measure the size of particles in the micron and submicron range in a solution. In DLS a laser is shone onto the sample causing a scattering in the light which is determined by the size and the movement of the particles. Through the measurement over time of the intensity of the light scattered, it is possible to estimate the size distribution of the particles in the sample.

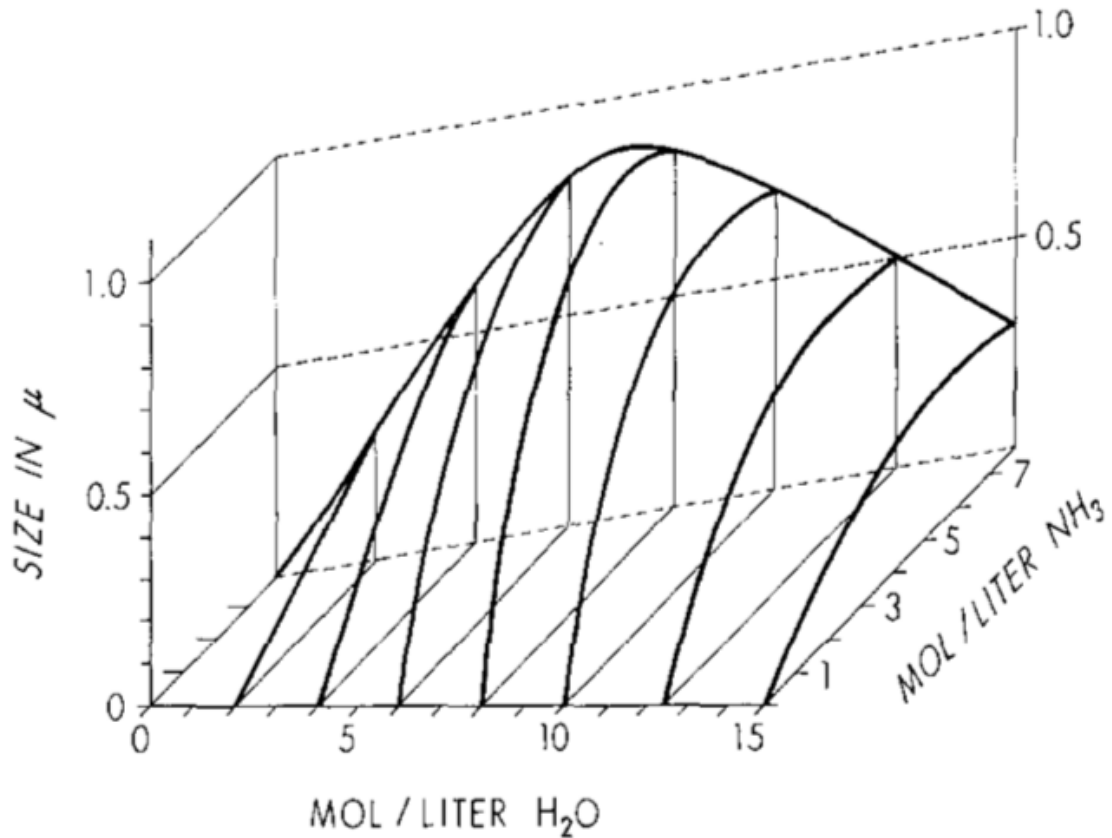


Figure 5.1: **Particle size of silica nanoparticles for TEOS 0.28 M based on concentration in H_2O and NH_3 adapted from the original Stöber paper [27].** This curve changes as higher or lower concentrations of TEOS are used or if other orthosilicates are used.

This technique can also be used to measure the ζ potential, or the surface charge and stability of the nanoparticles.

Some of the major limitations of DLS are the following:

- Limited Resolution and Sensitivity - DLS cannot discern particles by shape and so it cannot determine if a particle is spherical or amorphous. Further, DLS can only be used to analyze particles in the range between 1 nm and 100 μm .
- Homogeneity of the sample - DLS shows most of its limitation when the sample is not properly mixed into the medium. This leads to clumping which results in incorrect particle sizes, generally being too big with non gaussian size distribution.
- Density of the particles - If the density of the particles is too high in the sample, this can result in incorrect readings due to multiscattering.

5.2.2 BET Analysis

Brunauer-Emmett-Teller analysis also known as BET analysis is a method of measuring the surface area of a material with extremely high accuracy. The technique involves the use of Nitrogen gas as adsorbant, which attaches to the surface of the material. The pressure is monitored as the gas is adsorbed by the material, creating a relationship between the amount of adsorbant and the pressure in the chamber [29]. It is then possible to calculate the surface area of the samples from the pressure. An example of BET curve from the sample with the highest porosity (75% TMOS), is shown in figure 5.2.

Some of the major limitations of BET are:

- Homogeneity of the sample - BET assumes that the sample is homogeneous and so that the adsorbant is being uniformly distributed. Presence of contaminants or other materials might lead to an uneven distribution of the Nitrogen gas, resulting in inaccurate readings.
- Limited data - The only independent variable on which BET analysis relies is the pressure of the sample which means that the only information known is the quantity of adsorbant used. This limits the information we have to only knowing the surface area, which if it increases can be an indicator of porosity but that however does not give information about the pore structure and volume. Further, only relying on surface area can lead to misleading results since the particle's surface area might be changing not because of the presence of pores but due to other factors (such as bumps or structure change of the particle).

5.2.3 BJH Analysis

Barrett-Joyner-Halenda analysis or BJH analysis is instead a technique similar to BET but that focuses on measuring the pore volume and structure of the samples. BJH also studies the adsorption of gas as a function of pressure independently from the external area of the particle, however it focuses on determining the volume of the gas that is being adsorbed in the pores rather than calculating the surface area. This is an analysis method that is often done along with BET to have a better understanding of the sample's porosity and structure.

BJH shares the same major limitations that BET does.

5.2.4 UV-Vis absorbance analysis

Absorbance is the amount of light at a certain wavelength that a fluorophore can absorb. This is a quantitative value that depends merely on the concentration of the sample and it is not affected by other elements [20].

To analyze the absorbance, UV-Vis (Ultraviolet to Visible wavelength range) analysis is performed on 96 wells-trays in 70/30 Ethanol water. What the machine does is sending

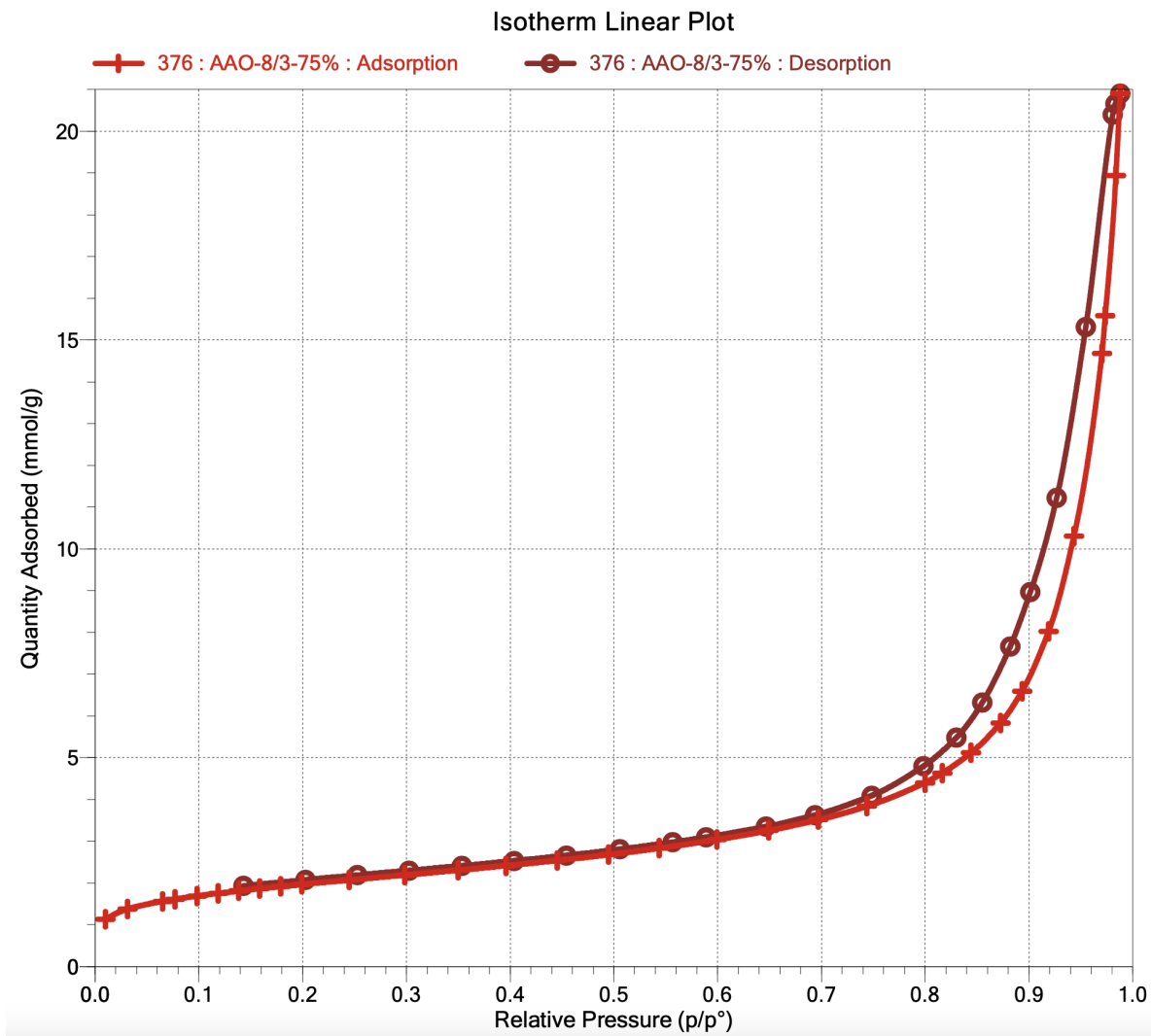


Figure 5.2: **BET Isotherm Linear Plot for highest porosity sample at 75% TMOS.**

light at a certain wavelength through the sample and measuring thanks to a detector the amount of light that reaches. It then compares the analyzed data to a blank or reference well and determines the effective amount that has been absorbed. In our case the quantities in each well were kept constant at $200 \mu\text{L}$ with a distance of 1 empty well from each sample, to prevent interference among the samples and the blank sample was filled with the same quantity of 70/30 Ethanol/water solution.

Some major limitations of UV-Vis analysis are the following:

- Specificity - UV-Vis is non specific, meaning that in case of heterogeneous samples, such as a particle with fluorophore, it doesn't distinguish what amount of light is being absorbed by the fluorophore or the particle. This means that this technique requires more controls to determine the approximate absorbance of the fluorescein

in the sample.

- Environmental interference - UV-vis requires a transparent plate to be able to detect the absorbance of the sample. This means that some of the light might get scattered, being absorbed by nearby samples. Thus, it is necessary to maintain a distance of 1 well from each sample. Further, all sample should be analyzed in the same medium and in the same quantity to have accurate results.
- Sensitivity - UV-vis has a limited sensitivity that doesn't allow it to be able to determine very small changes in absorbance. Thus it is necessary to calibrate the samples so that they are concentrated enough.
- Relative units - UV-vis uses relative units, which means that unless all the samples are measured at the same time and in the same conditions their raw absorbance cannot be compared. It is then necessary to have a calibration of the free dye over different concentration to be able to quantitatively convert the absorption of the samples into fluorophore concentration that can be compared with previous readings.

5.2.5 Emission Analysis

Emission or *Fluorescence* is instead the spectrum of released light from a fluorophore upon being excited. This can be a quantitative value for a known concentration of fluorophore, however due to its dependence to factors related to variations in its environment such as temperature, pH or , for our purposes, it can only be used qualitatively to assess the presence of fluorescence [20][31].

To measure the fluorescence of a sample, a light at an excitation wavelength is shone on the sample. If the sample emits any light back a detector perceives it and compares it to a blank to determine the fluorescence.

Similarly to UV-Vis analysis fluorescence analysis has the same major limitations. The only addition that should be done to fluorescence analysis' limitations is the fact that this is not a quantitative measurement, thus, it only indicates if the fluorescence is present or not.

5.2.6 SEM

Scanning Electron Microscopy is an imaging technique that can be used to visualize samples at a size of up to $\times 100,000$. The working principle behind this powerful method is to scan the sample through a moving beam of electrons. This beam can be regulated in intensity and size and interacts with the atoms producing backscattering of electrons, secondary electron and x-ray emission. These signals are detected by sensors in the vacuum chamber in which the sample is analyzed. The data recorded from the sensors is then used to form an enlarged image of the sample.

This method also permits to detect and highlight different materials if the sample is heterogeneous, being able to identify the presence of encapsulated dyes for example.

Some major limitations of SEM are the following:

- Conductive samples - SEM requires the samples to be conductive. If they are not, the samples need to be coated using carbon or iridium. This step can introduce artifacts if not performed correctly and might also change the sample.
- Cost - SEM is an expensive technique that requires trained personnel, making it often not usable for everyday analysis.

5.3 Duplicating the reaction

Using the Stöber method outlined in the original paper and previous literature [27][30], we synthesized 300 nm in diameter silica nanoparticles. This size was chosen with the idea of easily test and attach the particles to the fiber optic stub, however we did understand that smaller nanoparticles in the order of 50 nm would be more suitable for our application, as they would provide higher sensitivity of ions in the environment.

We used some training runs to familiarize ourselves with the standard procedure. After mixing together the reagents in the correct proportions we would let the samples on a shaker for at least 12 hours. After, we would proceed to wash the samples in ethanol to remove the excess ammonia left in the solution.

Due to their size, submicron particles are only mildly affected by gravitational sedimentation being instead strongly influenced by Brownian motion, which describes the random motion of the particles [32]. It is then necessary to use centrifuging to achieve a sedimentation and a proper washing of the samples. To target the centrifuging so that most of the nanoparticles in our range of interest are going to sediment we used Allen's calculation, [32][29], presented below.

$$\gamma = \frac{36}{\Delta\rho g d^{-\frac{5}{2}}} \left(\frac{2KT\eta}{3\pi t_f} \right)^{\frac{1}{2}}$$

where γ is the ratio of Brownian motion to settling motion, $K = k_b = \frac{R}{N_A}$, is Boltzmann's constant, $\Delta\rho$ is the difference in density of the liquid and the nanoparticles dispersed (Kg/m^3), g is the speed of the centrifuge in terms of gravitational accelerations (m/s^2), η is the dynamic viscosity of the liquid ($Pa \cdot s$), R is the universal gas constant ($J/(mol \cdot K)$), T is the temperature (K), t_f is the time of sedimentation for which the centrifuge runs (s), N_A is Avogadro's number and d is the critical particle diameter (m). To calculate the percentage of particles of size d that do not sediment in the solution, also known as quantity k , we use the following ratio:

$$k = 100 \cdot \frac{\gamma}{1 + \gamma} (\%)$$

The lower the k value, the more particles of that size will be found in the pellet after centrifugation. For our samples we kept the k value around 5 % to prevent aggregation and clumping. Further, redispersion was achieved only through vortexing, without the use of spatulas to prevent contamination and clumping.

5.4 Identifying the ideal concentrations

We tried to understand how the size and distribution of the nanoparticles varied based on differences in concentrations of water and ammonia as well as how the presence of ammonium hydroxide affected the reaction. To do so, we selected four points on the curve in Figure 5.1 and synthesized them twice: the first with high concentrations of ammonium hydroxide (high NH_4OH) and the second with half the amount of ammonium hydroxide (low NH_4OH). The results recorded through Dynamic Light Scattering (DLS) are displayed in Figure 5.3. On average it is possible to observe that for lower concentrations of ammonia and ammonium hydroxide the synthesis produces smaller particles and a more monodispersed solution.

Based on these observations, we identified 6M H_2O and 0.8M NH_3 as the ideal concentrations to produce the nanoparticles, to produce particles in our expected regime and with low polydispersity but also maintaining low the concentration of toxic reagents.

5.5 Adding porosity to the particles

One problem for which we couldn't use the nanoparticles produced using the regular Stöber procedure was that the synthesized product would be fully spherical particles. These being full and solid would not permit any encapsulation of fluorophore and the ions would not be able to enter the particles and interact with any fluorophore.

To solve this problem we decided to make the nanoparticles microporous, meaning that they contain pores of 2 nm or less in diameter according to ISO standards [33]. To achieve the microporosity we decided to use the aggregation property of the Stöber synthesis to our advantage by accelerating it. In this way, during the growth step the molecules don't have the time to arrange properly leaving gaps that create the porosity.

One of the main components that determines the speed of the reaction is the *ethyl* group of the orthosilicate TEOS. Thus, we decided to replace it with *Tetramethylorthosilicate* (TMOS), which being a smaller molecule due to the presence of the *methyl* group it reacts much faster as it is possible to deduct from the structures represented in figure 5.4.

5.5.1 Optimization of the porosity

To assess the effective changes that the addition of TMOS has on the reaction, we analyzed the produced nanoparticles' size, adsorption area (the area to which the adsorbent attaches [33]), porosity and pore size at different percentages of TEOS and TMOS in the orthosilicate mixture, maintaining a constant concentration of 0.27M. The results are reported in figures 5.5-5.6.

When referring to the percentage of TMOS in the orthosilicate solution we are referring to the molar percentage, following equation:

$$\%TMOS = \frac{C_{TMOS}}{C_{TMOS} + C_{TEOS}}$$

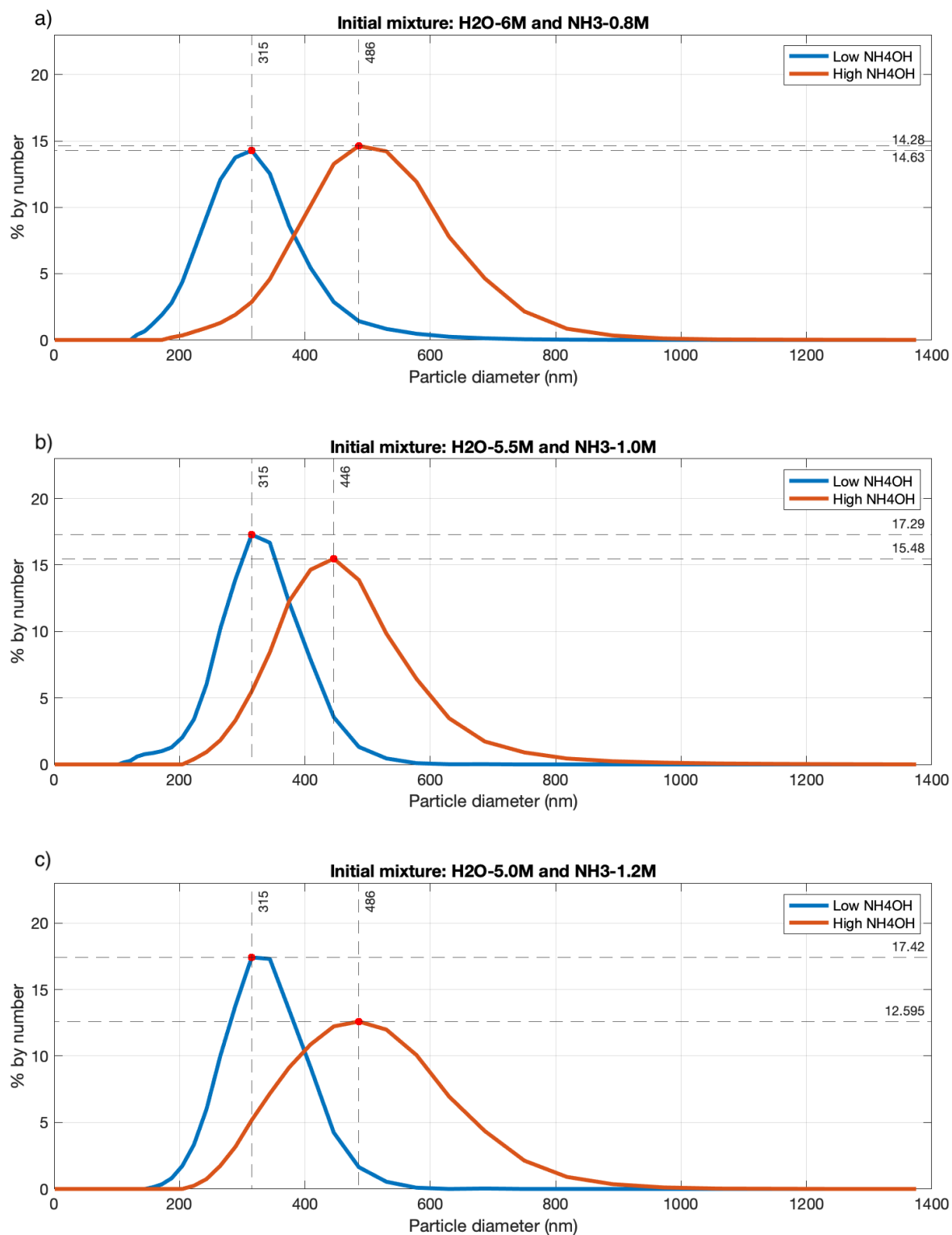


Figure 5.3: Size of 300 nm silica nanoparticles at different concentrations of H_2O and NH_3 with changes in size for high and low concentration of NH_4OH . As the concentration of Ammonium hydroxide is raised, it is possible to notice that the median diameter is about 100 nm larger and the distribution of the nanoparticles becomes more spread out. Maintaining low concentrations of ammonia and ammonium hydroxide, results in a production of smaller nanoparticles with a lower PDI.

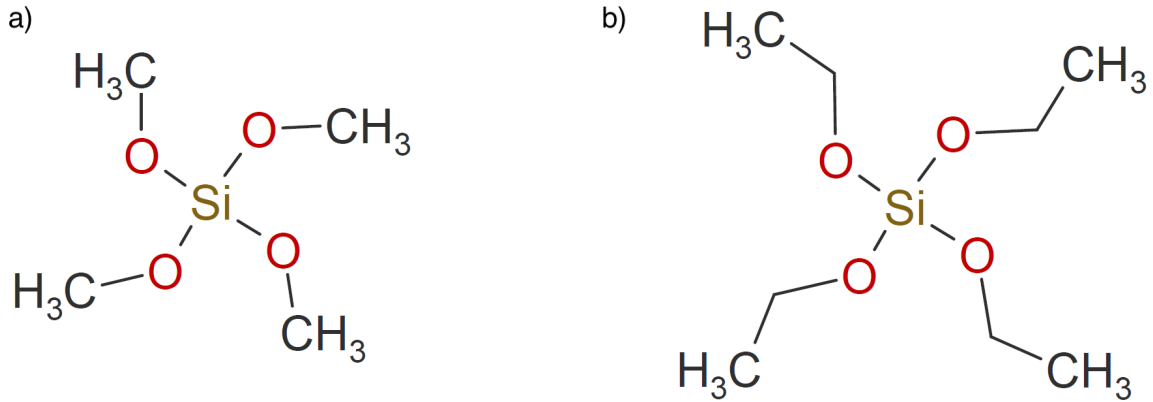


Figure 5.4: **Chemical structures for TMOS and TEOS [34].** On the right is presented the chemical structure of Tetramethylorthosilicate (TMOS) and on the right is presented the chemical structure of Tetraethylorthosilicate (TEOS). These molecules have very similar properties with the exception that TMOS has a higher reactivity due to the smaller size of the molecule, given by the methyl groups.

where C_{TMOS} and C_{TEOS} are respectively the concentrations of TMOS and TEOS, and their sum is constant (0.27M).

The porosity of a material can be determined in two ways:

1. As a ratio between the surface area measured by BET and the calculated one of a perfect sphere of the particles' diameter. Also known as Normalized Surface Area.
2. As a ratio of the pore volume measured by BJH and the volume of a perfect sphere of the particles' diameter. Also called porosity or porosity by volume. This is the most reliable way of determining the actual

The formula used to determine how porous the samples were by volume is the following:

$$Porosity(\%) = \frac{V_{pores}}{V_{pores} + \frac{1}{\rho}}$$

where V_{pores} is the volume of the pores and ρ is the density of silica.

As it is possible to notice, in figures 5.5a-e there is a non linear behaviour in all the properties. The sample seem indeed to suddenly increase in specific surface area (SSA), normalized surface area (NSA) and porosity by volume and decrease in size after a threshold of 60% TMOS. Further at 80% TMOS, the porosity by volume and NSA seems to reach a maxima and then starts decreasing. Analyzing in smaller steps the gap between 60% and 80% TMOS we noticed that a peak in porosity by volume is present at 75%.

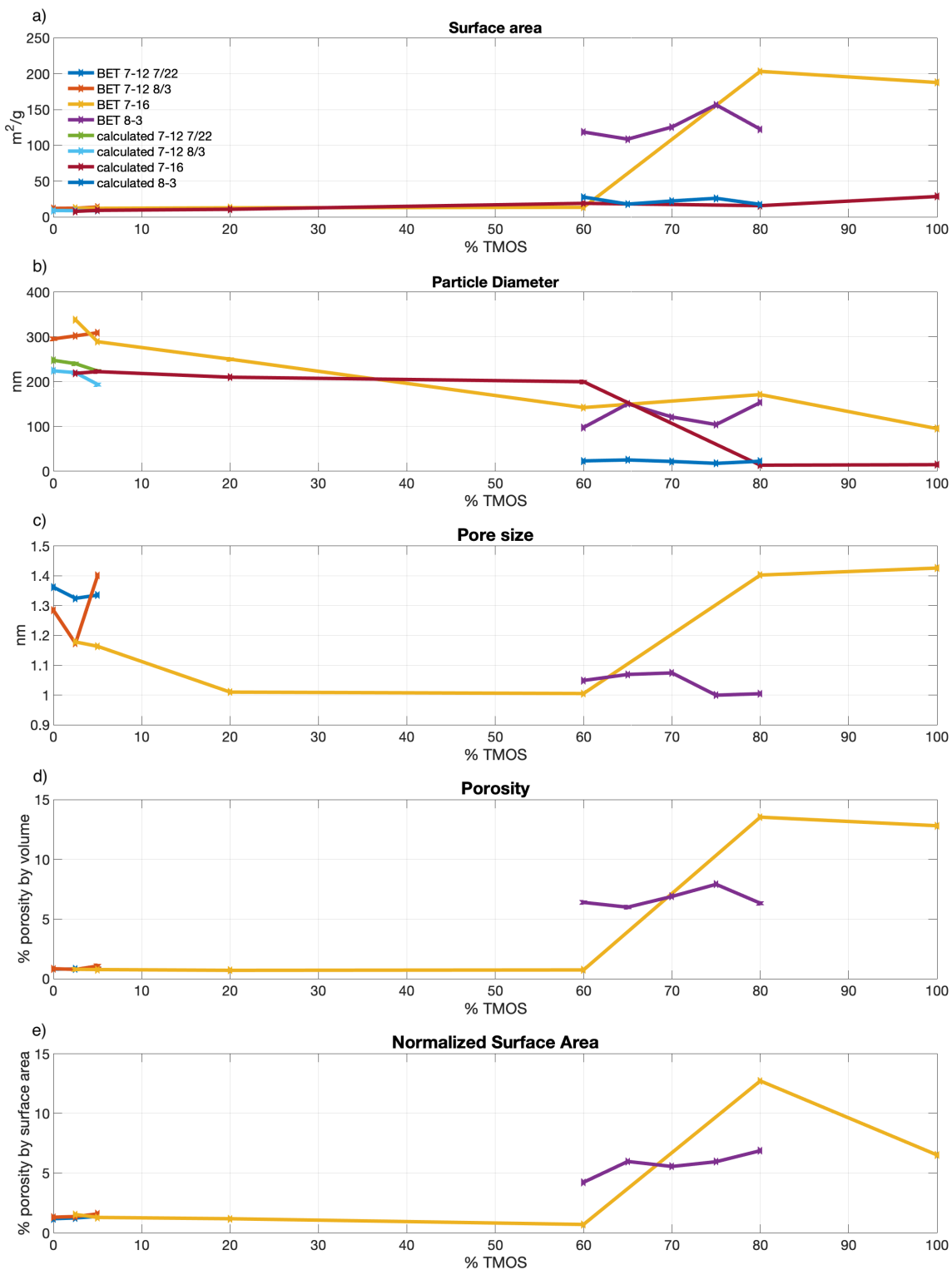


Figure 5.5: Particle properties for different quantities of TMOS and TEOS. a) Specific surface area (SSA) of the nanoparticles for different percentages of TMOS, measured using BET and calculated with spherical approximation from

Figure 5.5: DLS data. b) Particle diameter calculated from BET and compared with DLS data. c) Pore diameter measured from BET data only d) Porosity calculated from BJH data. e) Normalized surface data calculated from BET data with respect to DLS data.

After looking at the samples under SEM, as presented in figure 5.5f it was observed that the presence of TMOS didn't add porosity until 60% but only made the particles smaller, presumably due to the fact that TMOS starts hydrolyzing first, using TEOS molecules as nuclei. Being TMOS in lower concentration, it then creates quickly a porous core for the nanoparticle. The remaining TEOS in solution however grows on the porous nuclei with slower speed, filling the gaps and removing the porosity.

With a majority of TMOS (in the region between 60% and 80% TMOS), the nanoparticles are mostly porous due to the quick formation of porous cores. However, it is then thanks to TEOS that the silica doesn't become amorphous. TEOS due to its slow reactivity gives spherical structure by filling some of the pores and reducing their size. This also prevents the particle from becoming amorphous due to a too fast reaction by too high concentration of TMOS. Amorphous silica is indeed formed when only TMOS is used in the synthesis, making the presence of particles totally absent.

From the gathered data, it was then determined that 75% is the ideal percentage of TMOS to produce highly microporous and monodispersed silica nanoparticles.

5.6 Encapsulation of fluorophore

Once we modified the Stöber procedure to produce reliably highly microporous 300 nm silica nanoparticles, we started to encapsulate fluorophores to understand the effect of the particle on the properties of the dye.

Fluorescein is an inexpensive and innocuous dye that is sensitive to Ph changes and that is 7Å in size. It is then a convenient candidate to study the changes in its properties once encapsulated. In this way we can also understand how more expensive analyte sensitive fluorophores might behave once encapsulated without sacrificing too much material. Another advantage is that fluorescein is relatively strong

To add the fluorescence to the nanoparticles, the dye was added in the desired concentration to the ethanol and the solution was then used as the main mixture for the synthesis. In this way the silica would grow around the fluorescein molecules fully encapsulating them in equal concentration in each particle.

To characterize the changes that the encapsulation brought to the properties of fluorescein compared to its free counterpart, we gave particular attention to the changes in absorbance and fluorescence. These are indeed key properties necessary for the quantitative modulation of the light signal injected in the probe that needs to be sent back.

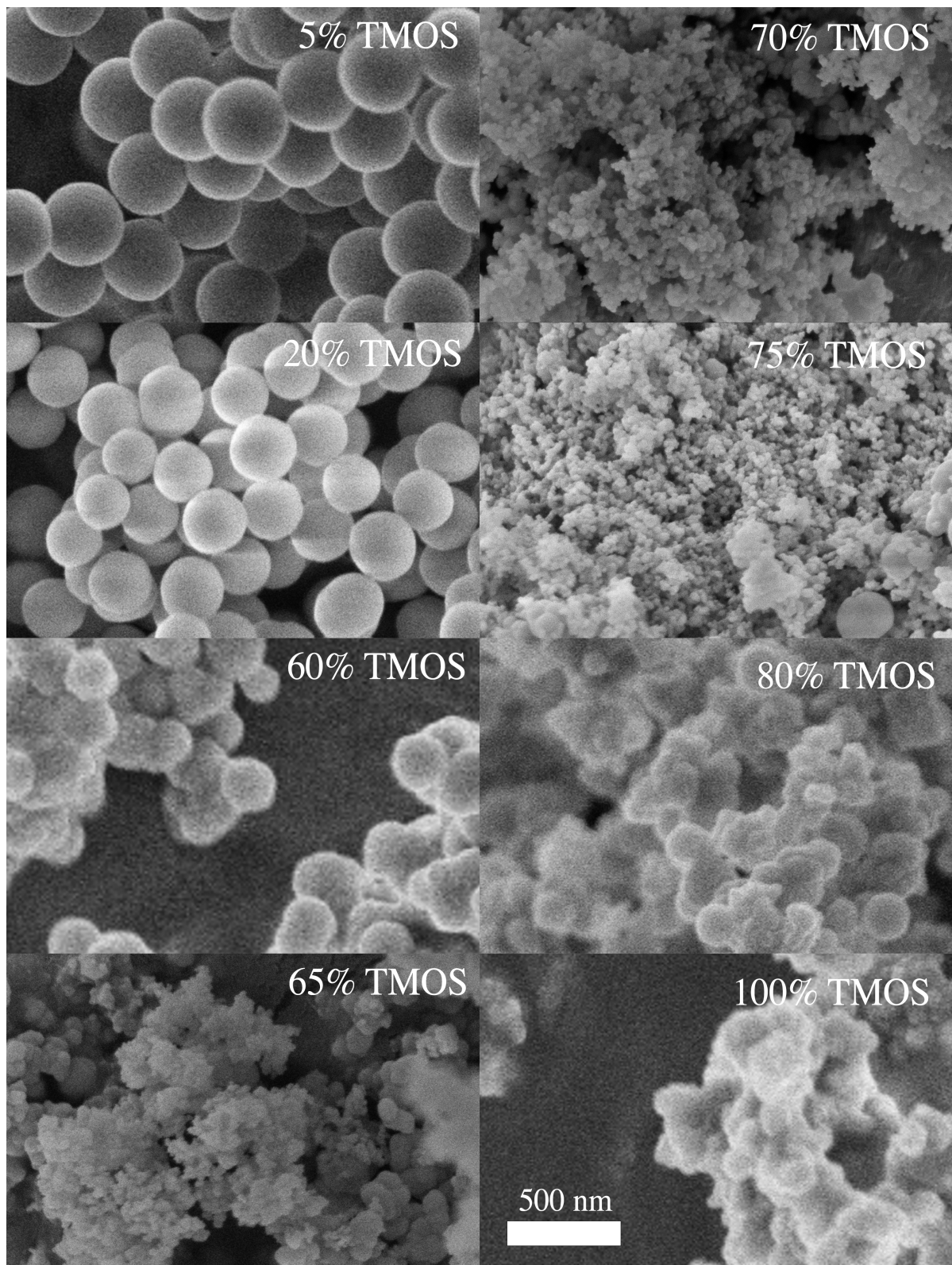


Figure 5.6: SEM images of the particles at different TMOS percentages.

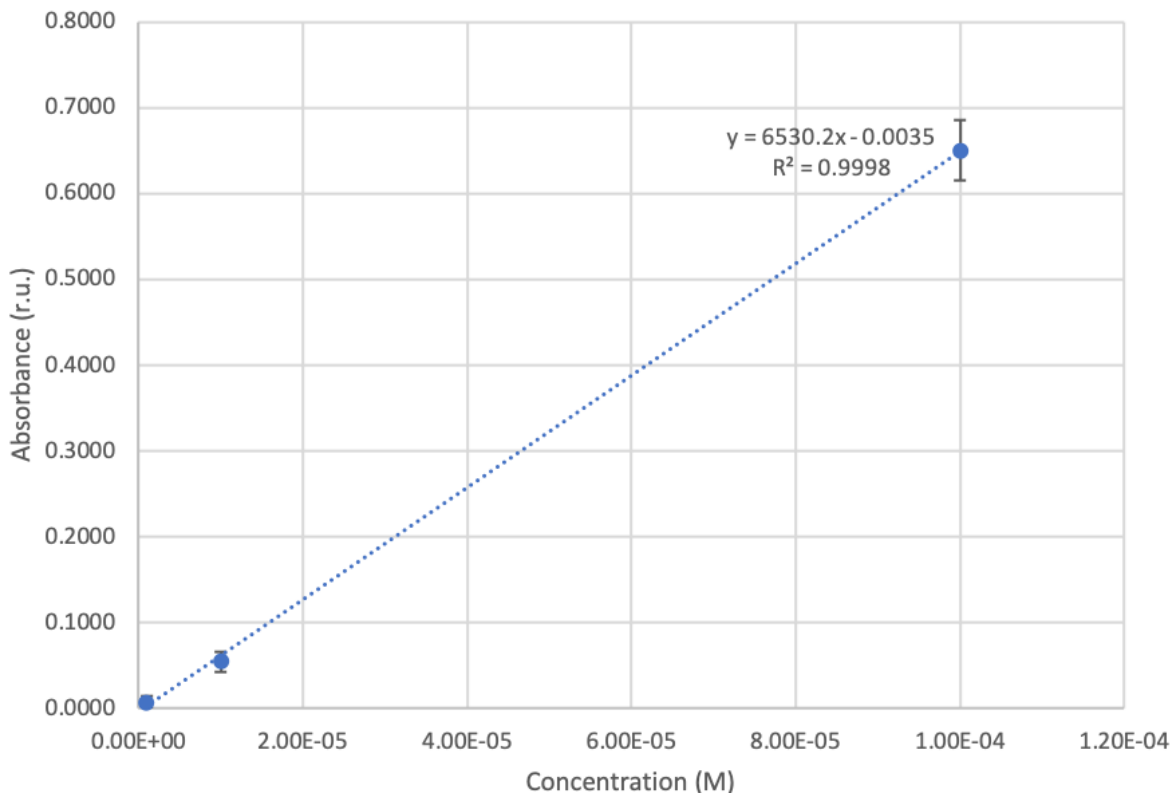


Figure 5.7: **Beer-Lambert relationship for fluorescein.** The analysis was performed with increments of order from 10^{-3} M to 10^{-7} M. The Absorbance would only be linear until 10^{-4} M making this the ideal concentration to be used within the nanoparticles since it's the upper limit for which Beer Lambert's law persists. In this way, the particles will retain at maximum this concentration meaning that the whole absorbance analysis can be performed based on a linear relationship.

5.6.1 Absorbance Analysis

Absorbance was used to calibrate the ideal concentration of fluorescein to be encapsulated based on Beer-Lambert's law. In the region indicated by this law there is a linear relationship between the concentration of the dye and its absorbance. This relationship holds until a critical concentration after which *self quenching* and other molecule interactions start affecting the absorption, making the relationship not linear[20]. Self quenching is an effect that manifests due to high concentrations of fluorophores. During this phenomena energy is transferred in a non radiative way among the same molecules causing a decrease in emission intensity. For fluorescein, the Beer-Lambert's relationship was observed in figure 5.7 and 10^{-4} M was determined to be the highest concentration for which the law would hold.

It is important to notice that the particle itself increases the overall absorption of the solution due to its large volume compared to fluorescein. Thus to have a good estimation of the absorption of the fluorophores it is necessary to have a control reference of only

silica nanoparticles in the same concentration. This is a good approximation, however, presence of even few clumps or aggregates can affect the absorbance and its standard deviation. This variation in absorbance is minimal when the fluorophore is present since its signal is stronger due to the high molar absorption of fluorescein ($75000 \text{ M}^{-1} \cdot \text{cm}^{-1}$) which is much larger than the molar absorption of silica ($1\text{-}10 \text{ M}^{-1} \cdot \text{cm}^{-1}$). However while the dye is absent the absorbance is much more sensitive to the differences in concentrations of silica, which can result in negative reading with a larger standard deviation due to the presence of small aggregates.

5.6.1.1 Determining the concentration of fluorophore

When recording the absorbance of the particles with the fluorophores it is then important to also measure the same type of particles without the dye (also called control) and to take the absorbance of the standards to recreate the curve in figure 5.7. In this way, by subtracting the absorbance of the sample from the control, it is possible to correctly approximate the concentration of fluorescein that is absorbing the light and compare it to the initial concentration added to determine the encapsulation efficiency.

5.6.2 Results of the encapsulation

After analyzing the nanoparticles' absorbance we noticed that the concentration of fluorophores in the final solution would be estimated to be about 40% of the initial after 7 rounds of washes. However, when repeating the recordings with the same samples after 60 days and rewashing the samples 3 times with lower amounts of ethanol removed, compared to newly produced ones, no fluorophore was detected by the absorbance as shown in figure 5.8. Further, over washes, the concentration of fluorophores would slowly decrease initially, however after the wash was repeated after 60 days, there was an increase in concentration of removed fluorophores as shown in figure 5.9.

Both results indicate that the fluorescein is leaking from the particles, leading to a decrease in absorbance values. The fluorophores in the nanoparticles, over washes, are indeed subjected to a chemical gradient towards the outside that increases the fewer fluorescein is present outside of the nanoparticles. Since the pores are about the size of fluorescein, this creates a leakage which is barely noticeable but that is sustained over time and can be accelerated through centrifuging.

5.6.3 Double encapsulations

To prevent the fluorescein from leaking we decided to encapsulate the nanoparticles in a shell fabricated with the same procedure used for the porous particles, adding the latter in the ethanol solution.

The TMOS/TEOS mixture was kept at 75% TMOS in molar ratio since that was the critical point at which the silica produced the highest porosity and smallest diameter pores. Our expectations were that the low amounts of orthosilicate mixture would create

a porous shell and reduced in size even further the pores by aggregating on the surfaces already formed and trapping even further the fluorescein.

We prepared samples at increments of 0.025 M of orthosilicate mixture reaching at maximum 0.1 M and adding a sample at 0.01 M to observe the change at one increment of distance in concentration. For each sample an equivalent control without fluorescein was produced to estimate the amount of absorbance only from the dye. One sample without shell was also prepared and centrifuged along with the other shell sample to compare its final concentration of fluorescein and the results are plotted in figure 5.10.

According to absorbance readings, after 12 washes the samples without a shell lost all of their fluorophore (figure 5.10a), however they still had some mild fluorescence (figure 5.10b).

The samples with a shell on the other hand seem to retain fluorescein much better with an increasing trend peaking at 0.025 M of TMOS/TEOS mixture as it is notable from both absorption and emission readings (figure 5.10). 0.025 M was then determined to be the critical concentration at which the shell is neither too thin nor too thick and the fluorophores are trapped without being fully covered by the silica.

Looking at the DLS analysis presented in figure 5.11 it is possible to notice that the size of the silica nanoparticles remains approximately the same (between 200 and 300 nm) with an increasing trend, until at 0.075 M where a spike of smaller nanoparticles is detected.

Our interpretation is that, the newly added orthosilicate mixture builds upon the old particles until reaching the critical size of 300 nm (limited by concentration of Ammonia and water) after which it starts growing inside of the pores making them smaller.

However, Once the nanoparticles have reached the critical size and all the pores have been filled not allowing light to reach the encapsulated fluorophores, the orthosilicate in excess forms new nuclei upon which new nanoparticles grow. The size of these new porous particles is then limited by the leftover TMOS/TEOS mixture and it is clear in the peak of 100 nm nanoparticles in the 0.075 M.

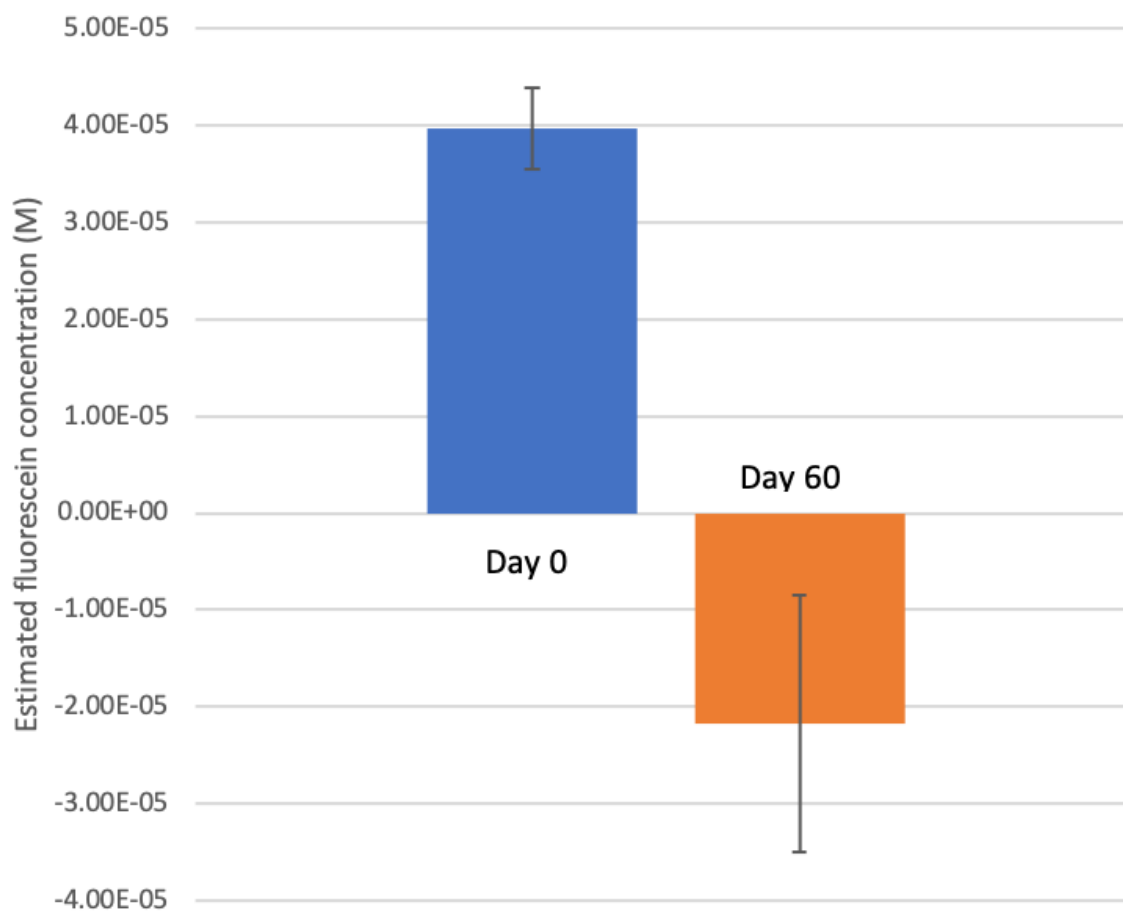


Figure 5.8: **Estimated fluorophore concentration in the nanoparticles based on absorbance analysis.** The nanoparticles were initially produced with 10^{-4} M fluorescence, after 7 washes they had an estimated absorbance equal to about 40% the initial. After 60 days and 3 washes, the absorbance of the control was in most cases higher or close to the one of the samples with fluorescein, causing negative results. The results were taken over three readings from the same sample on both days.

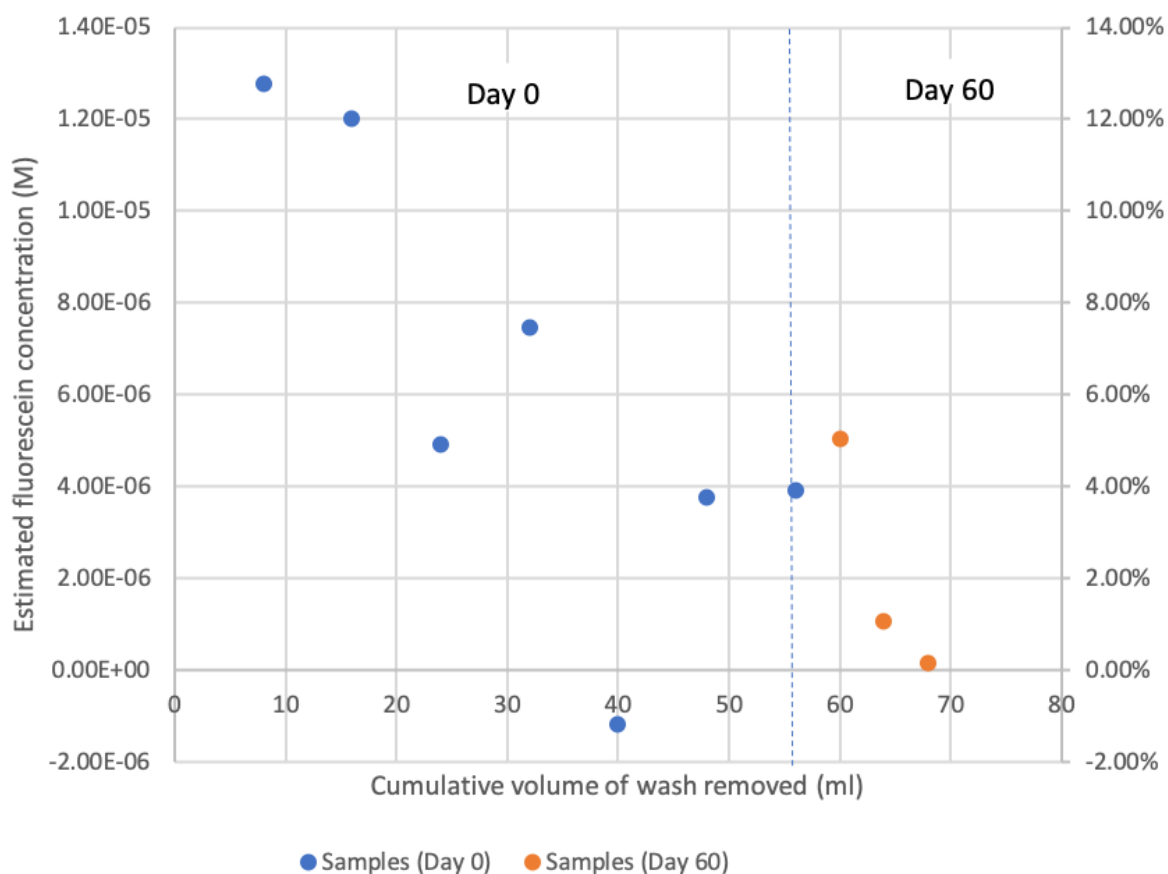


Figure 5.9: **Concentration of fluorescein removed over wash.** As the samples are being washed, the concentration of fluorescein removed decreases non linearly, remaining below 5% in the last 3 readings on the first day. At the 60th day when the washes are being repeated, there is a higher concentration of sample being removed while after, the concentration removed remains negligible. This hints to a constant leakage of fluorophore from the particles that accumulated over time.

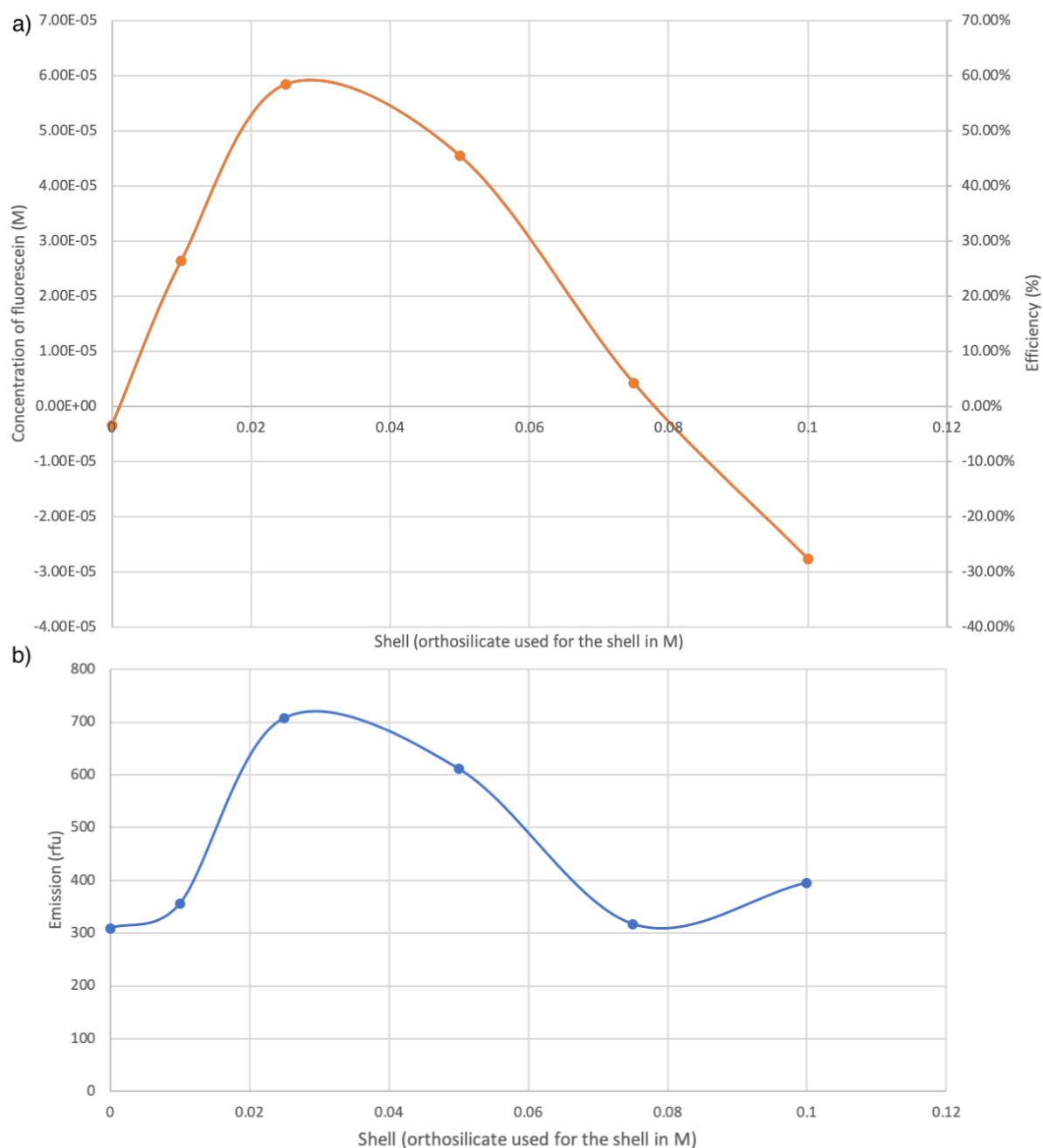


Figure 5.10: **Behaviour of fluorescein in nanoparticles with shells produced over concentrations of orthosilicate.** a) Presents the concentration of fluorescein estimated through absorbance readings. The sample at 0.1 M is particularly negative due to the very low molar absorption of silica which amplifies the small oscillations in sample concentration. b) Emission of the samples after subtraction from silica controls.

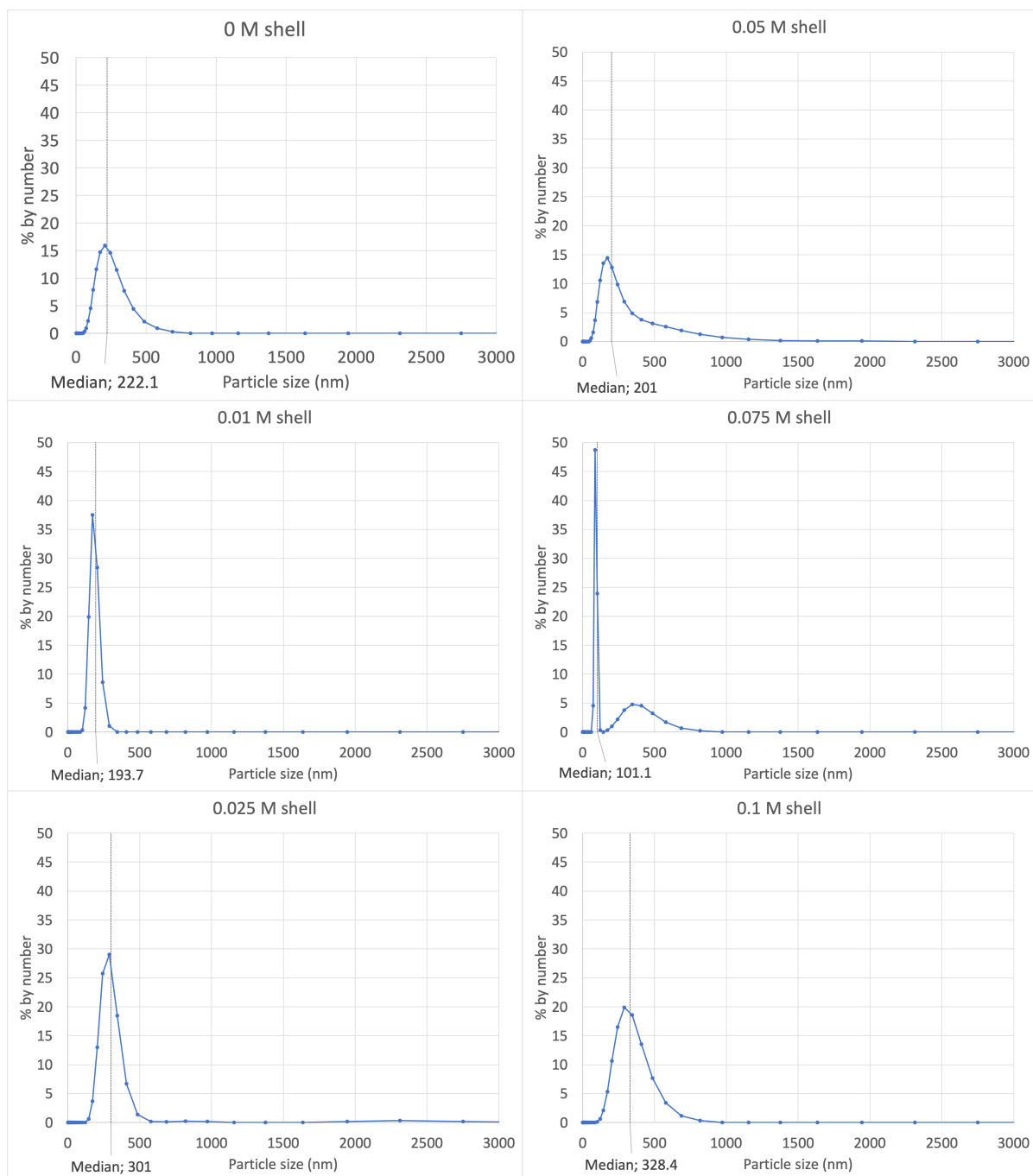


Figure 5.11: Dynamic Light Scattering analysis of particles size based on shell orthosilicate mixture concentration (written on top).

Chapter 6

Discussion

The goal of this thesis was to develop a sensor capable of modulating light based on its environment for in vivo and in vitro brain experiments, so that it could be interfaced with the optic endoscope designed by Gangarosa [2].

The sensor needed to be biocompatible, effective, and localized. It also had to reduce the photobleaching rate of encapsulated fluorophores, permit co-localization and FRET excitation among the dyes, and limit the analyzed space to the extracellular matrix.

Such a sensor is crucial for high spatial and temporal monitoring of molecular dynamics in localized areas of the brain in both in vivo and in vitro studies. Analytes like oxygen and potassium are key players in diseases such as epilepsy and spreading depression. Being able to study their changes in real-time could open the doors to new research towards a cure and better understanding of our brain.

Further, this technology can be translated to other research fields and analysis, since the sensor can be fully customized this allows a broad set of applications, ranging from food safety, environment monitoring to industrial monitoring.

We began by replicating the Stöber procedure to synthesize fully spherical, monodispersed silica nanoparticles with a diameter of 300 nm. This method is reliable and can be scaled easily, facilitating its translation to industrial manufacturing. The particles consist of silica, a biocompatible material that can also bind to glass through the use of a silane coupling agent. This allows the sensor to be directly attached to the fiber stub through a covalent bond, facilitating easy interfacing with Gangarosa's optic endoscope.

Next, we modified the synthesis process to create highly porous particles by adding TMOS. Due to its methyl group, this orthosilicate accelerates the aggregation reaction in the synthesis, resulting in pores within the particle and increased porosity. High porosity is essential for encapsulating more fluorophores in the particles and enabling their interaction with ions. It is also crucial to ensure that the pore size is smaller than the fluorophores to prevent leakage. We analyzed the changes in porosity and size as a function of the TMOS percentage in the orthosilicate mixture and observed that the particles became highly microporous (pores <2nm) and smaller at 75% TMOS.

Found the ideal ratio of the orthosilicate mixture, we used fluorescein to test how

encapsulation affected the properties of the fluorophores. Through absorbance analysis, we found that older samples exhibited no fluorophore absorbance. This suggested that the dye was leaking from the particles, possibly due to its size being similar to that of the pores (about 1 nm).

To address the leakage issue, we synthesized a shell on top of the particles with encapsulated dye using the same Stöber procedure at 75% TMOS. We then varied the concentration of the orthosilicate mixture to control the shell thickness and observed the changes in absorbance and emission. We found that a peak in absorbance was present for particles with a shell of 0.025 M TMOS/TEOS mixture after multiple washing steps. This result indicated that at this concentration, the shell was thick enough to prevent fluorophore leakage without completely occluding the pores, thus blocking the light from reaching the fluorophores while maintaining an efficiency of 60% absorbance compared to the free dye.

Overall, we successfully synthesized fluorescent porous silica nanoparticles that are biocompatible, customizable, and capable of containing with good retention (about 60% by absorption) multiple fluorophores. These nanoparticles prevent fluorophore leakage, restrict analysis to the extracellular matrix, and can be covalently bound to fiber optics for easy utilization with an external system. Our sensor meets the desired criteria, offering a valuable tool for investigating molecular dynamics in localized brain areas and providing a platform for further research in a variety of fields.

6.1 Advantages compared to previous systems

Compared to previous systems our particles permit an integration of features that before could only be seen individually:

- Our particles are **biocompatible**, **customizable** and **do not leach fluorophores**, maintaining **high fluorophore absorbance efficiency**.
- Our system allows **multiplex analysis** of analytes, limited only by the emission and absorbance spectrum of the encapsulated fluorophores.
- The binding of the particles to the fiber optic restricts the **analyte monitoring locally** maintaining **high resolution** in the analysis temporally and spatially.
- Our particles are designed to be used to **ratiometrically determine** the concentration of analytes. Previous systems are mostly used only for intracellular staining, without full control on the location.
- this synthesis is **cheap**, **stable**, **sustainable** and **scalable** allowing plenty of applications even outside of the biomedical field compared to other systems.

6.2 Impact

6.2.1 Economic / Manufacturability / Technology Transfer

The cost of the materials and tools used in the Stöber procedure is economical and the procedure can be scaled maintaining the same yield and without side effects, allowing an easier transition to industrial production with low costs per production unit. The characterization of the nanoparticles is however costly due to the required specific equipment, such as BET, UV-Vis Absorbance measure, Fluorescence machine and SEM.

6.2.2 Environmental/ Sustainability

The synthesis of the silica porous nanoparticles was designed considering also its impact on the environment, using low to nontoxic reagent and using low concentrations of ammonia to reduce the danger of the waste. Further, the Stöber procedure does not require any large amounts of energy keeping the process sustainable and environmentally friendly. Finally the nanoparticles can be engineered to be used for pollutant detection or environmental changes to help with the issue of global warming.

6.2.3 Ethical

These nanoparticles are intended to be used for animal studies to monitor the concentration of multiple analytes in localized areas in the extracellular matrix. However, the knowledge obtained from such studies can be applied and translated also to humans as well allowing us to benefit from it.

6.2.4 Health and Safety

The nanoparticles to be used in animal studies need to be FDA approved. This might result challenging, however, other systems using silica nanoparticles have been approved in the past (C-DOTS in the specific[13]), making it easier for our project to also be passed in case we wanted to use the particles in animal studies. Further, the procedure uses reagents that are minimally dangerous, making it a safe process. It must be taken into consideration that when the particles are dried and made into a powder, they are very fine and may cause health problems if inhaled.

6.2.5 Social / Political / Global

As specified in the Health and Safety section, the nanoparticles if applied for animal testing will need to comply to multiple regulations, including NDA but also others related to waste disposal, patent and environment. Further these particles can be redesigned for other applications that can vary widely and in this way influencing other sectors, having a global impact. In our case, such particles can help develop new treatments also against neurodegenerative diseases having thus a global health impact.

6.3 Optimization and Future Direction

In this study we did not observe the effects that the encapsulation has on the photobleaching rate of the fluorophores compared to when they are free. It would be interesting to observe if the limited movement of the fluorescein due to the silica, also reduces the rate at which it photobleaches, allowing longer recordings in studies. Another consideration to be made is that the particles have not been tested with analyte-specific dyes. Thus it is important to understand if the encapsulation also limits the sensitivity of the fluorophores to the analytes.

A future improvement that could be done to the system would be to wash the particles in Ethanol with fluorescein at the used concentration. In this way, since the dye can leak from the particles, there would not be leakage due to the chemical gradient pushing the molecules towards the regions of lower concentration. This would hypothetically allow the particles to retain higher concentrations of the fluorophore during the shell formation.

Encapsulation of multiple dyes should also be considered to observe if FRET excitation still persists from within the particle. Finally, using the appropriate dyes, it would be important to test the sensor when connected to the fiber stub with the Optic Endoscope.

Chapter 7

Conclusion

Overall, we managed to produce fluorescent porous silica nanoparticles using a modified Stöber procedure that contains 75 molar% TMOS in the orthosilicate mixture with TEOS. Fluorescein was used to measure the change in fluorophore properties once encapsulated in the particles, however leakage of the dye was observed from the particles. Adding a shell to restrict the size of the pores was an efficient solution that allowed an absorbance efficiency of 60% compared to the free dye and to the particles without shell. Consequently, our particles have shown their ability to locally restrict the position of the fluorophores. This brings many advantages compared to previous systems, including the possibility of monitoring multiple parameters simultaneously, the possibility for FRET excitation and the high spatial and temporal quality in the recordings. Future steps to continue this research would be to study the effects of the encapsulation on the photobleaching rate and testing the particles with an external system such as the one designed by Gangarosa [2]. Finally, this is a very versatile technology that can be applied and should be translated to multiple fields and offering many advantages on different current research challenges compared to other current technologies.

Appendix A

Codes

1. **HighKSim.m** - Code used to simulate using the Hodgkin-Huxley model the changes in membrane potential in a neuron during an action potential. The model is able to simulate based on a range of factors such as extra and intracellular levels of ions, time and can even consider stimulation of the neuron through addition of current.
2. **Plot_particle_distribution.m** - Code used to elaborate data received from DLS analysis. To use, run the code in the same folder with the .csv files, define number of rows and identify key values (Standard deviation, PDI, median and beginning of data) and the code will plot the distribution of the particles, calculate the density for each particle size and identify whether the solution is mono or polydisperse.
3. **ExtractFluorescence.m** - Code used to extract the fluorescence spectrum from the recorded fluorescence data. To use, run the code defining the file with the data and the number of rows analyzed. The code will plot the curve for each well, subtract the blank (by default wells A1-A3) and determine the peaks of each curve, averaging samples by row in groups of 3.

HighKSim.m

Created by: Alessandro Ascani Orsini

Date: 3/23/2023

Description: This code simulates the changes in action potential, current and gating variables in a neuron given ionic concentrations

Contents

- [Clean everything](#)
- [Settings](#)
- [Prepare data](#)
- [Calculate AP dynamic](#)
- [Run simulation using euler's method](#)
- [Plot results](#)

Clean everything

```
close all;
clear all;
clc;
```

Settings

Inputs

```
imgtitle = 'a';
Cm = 1; % membrane capacitance (uF/cm^2)
Vi = -70; % resting membrane potential (mV)
Iapp = 0; % applied current (uA/cm^2)
dt = 0.0001; % time step (ms)
t = [0, 20]; % simulation time (ms)
T = 278; % temperature (K)

% Ion concentrations
Kin = 140; % intracellular concentration of K+ (mM) (typically 140 mM)
Kout = 4; % extracellular concentration of K+ (mM)(typically 4 mM)
K05 = 4; % typical extracellular concentration of K+ (mM) for which the channels are half open
Nain = 15; % intracellular concentration of Na+ (mM)(typically 15 mM)
Naout = 145; % extracellular concentration of Na+ (mM)(typically 145 mM)
Na05 = 145; % typical extracellular concentration of Na+ (mM) for which the channels are half open

% Ideal driving forces
ENa = 55; % reversal potential of Na+ channel (mV) - reference
EK = -72; % reversal potential of K+ channel (mV) - reference
EL = -50; % reversal potential of leakage channel (mV)

% Channel conductance
gNamax = 120; % maximum conductance of Na+ channel (mS/cm^2)
gKmax = 36; % maximum conductance of K+ channel (mS/cm^2)
gL = 0.3; % maximum conductance of leakage channel (mS/cm^2)
z = 1; % ionic valence of ions (K+ and Na+ both have +1)

% Constants
R = 8.314; % gas constant (J/(mol*K))
F = 96485.3321; % Faraday's constant (C/mol)

% Functions
Ex = @(X_in, X_out,T) ((R.*T)./(z.*F)).*log(X_out./X_in).*1e3; % Nernst equation for potential (V)
```

Prepare data

Preallocate arrays

```
t = t(1):dt:t(2);
Vm = zeros(1,length(t));
m = Vm;
h = m;
n = m;
IK = m;
INa = m;
IL = m;

% Initial gating conditions
Vm(1) = Vi;
m(1) = 0;
n(1) = 0;
h(1) = 0;
```

Calculate AP dynamic

Calculate driving potentials

```
ENa = Ex(Nain,Naout,T);
EK = Ex(Kin,Kout,T);

% Adjust permeability
gX = @(Xin,Xout,gmax,X05) gmax.*(Ex(Xin,Xout,T)./Ex(Xin,X05,T)); % make conductance change from typical
gK = gX(Kin,Kout,gKmax,K05);
%gK = gKmax;
gNa = gX(Nain,Naout,gNamax,Na05);
%gNa = gNamax;
```

Run simulation using euler's method

```
for i = 2:length(t)
    % Calculate gating parameters alpha and beta
    a_m = 0.1.*(Vm(i-1)+40)./(1-exp(-(Vm(i-1)+40)./10));
    b_m = 4.*exp(-(Vm(i-1)+65)./18);
    a_h = 0.07.*exp(-(Vm(i-1)+65)./20);
    b_h = 1./(1+exp(-(Vm(i-1)+35)./10));
    a_n = 0.01.*(Vm(i-1)+55)./(1-exp(-(Vm(i-1)+55)./10));
    b_n = 0.125.*exp(-(Vm(i-1)+65)./80);

    % Calculate gating variables
    m(i) = m(i-1)+dt.*(a_m.*(1-m(i-1))-b_m.*m(i-1));
    h(i) = h(i-1)+dt.*(a_h.*(1-h(i-1))-b_h.*h(i-1));
    n(i) = n(i-1)+dt.*(a_n.*(1-n(i-1))-b_n.*n(i-1));

    % Calculate current
    INa(i) = gNa.*m(i).^3.*h(i).*(Vm(i-1)-ENa);
    IK(i) = gK.*n(i).^4.*(Vm(i-1)-EK);
    IL(i) = gL.*(Vm(i-1)-EL);

    % Update membrane potential
    Vm(i) = Vm(i-1)+dt.*(1./Cm).*(Iapp-INA(i)-IK(i)-IL(i));
end
```

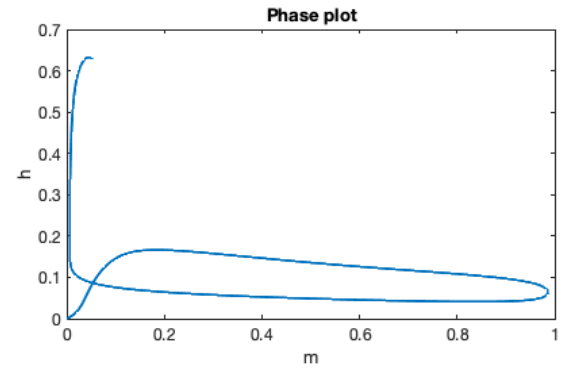
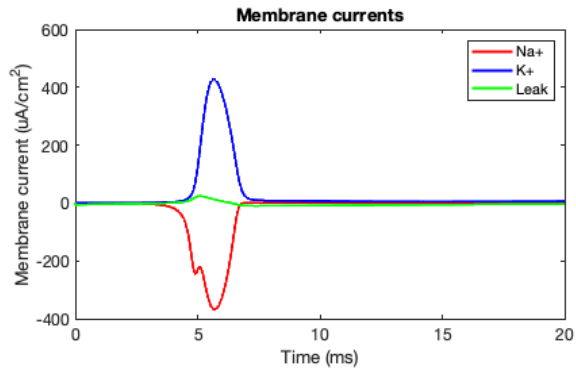
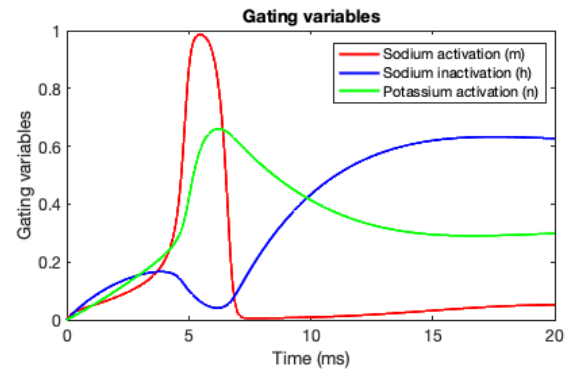
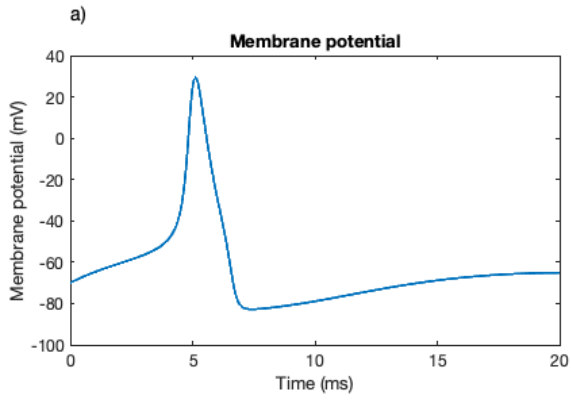
Plot results

```
myFigure([15 9]);
tha = sgtitle(imgtitle);
tha.HorizontalAlignment = 'left';
subplot(2,2,1);
plot(t, Vm, LineWidth=2);
xlabel('Time (ms)');
ylabel('Membrane potential (mV)');
title('Membrane potential');

subplot(2,2,2);
plot(t, m, 'r', t, h, 'b', t, n, 'g', LineWidth=2);
xlabel('Time (ms)');
ylabel('Gating variables');
title('Gating variables');
legend('Sodium activation (m)', 'Sodium inactivation (h)', 'Potassium activation (n)');

subplot(2,2,3);
plot(t, INa, 'r', t, IK, 'b', t, IL, 'g', LineWidth=2);
xlabel('Time (ms)');
ylabel('Membrane current (uA/cm^2)');
title('Membrane currents');
legend('Na+', 'K+', 'Leak');

subplot(2,2,4);
plot(m, h, LineWidth=2);
xlabel('m');
ylabel('h');
title('Phase plot');
```



Plot particle distribution

Created by: Alessandro Ascani Orsini

Date: 6/30/2022

Description: This code selects all the csv files in the folder and opens them, plotting the particle size and distribution of each.

Contents

- [Clean everything](#)
- [Settings](#)
- [Import the tables](#)
- [Check if monodisperse](#)
- [Plot](#)
- [Particle concentration in the samples](#)

Clean everything

```
close all;
clear all;
clc;
```

Settings

```
table_s = 50; % where the data recorded table starts
sd = 10; % where to find the standard deviation value
pdi = 11; % where to find the polydispersity index
part_median = 27; % where to find the median of the particles
rw = 1; % number of rows
figName = 'Particles Size with different M of fluorescein.'; % name that the figure will have
% particle density
porosity = .127249; % porosity of the sample
v = @(r) (1-porosity).*4.*pi.*(r).^3./3; % volume of a sphere
massE = 0.31962; % mass expected of the silica sample (calculated) (g)
dsio2 = 2.65; % density of silica (g/cm^3)
vf = 0.020; % final volume where the particles are dispersed (l)
```

Import the tables

```
files = struct2cell(dir('*.csv')); % first, finds all the csv files
figure(Name=figName)
for i = 1:size(files,2) % for each file
```

```
names = files{1,i}; % get the names of the file
tables = table2array(readtable(names)); % extract the table
data_t = tables(table_s:end,:); % table with raw data
[mx,my] = max(data_t(:,2)); % get maxima coordinates
```

Check if monodisperse

```
fprintf([names, '\n']);
if tables(pdi,3) < 0.1
    fprintf('Monodisperse \n');
    line_c = 'g';
else
    fprintf('Polydisperse \n');
    line_c = 'r';
end
```

```
Cnum.csv
Polydisperse
```

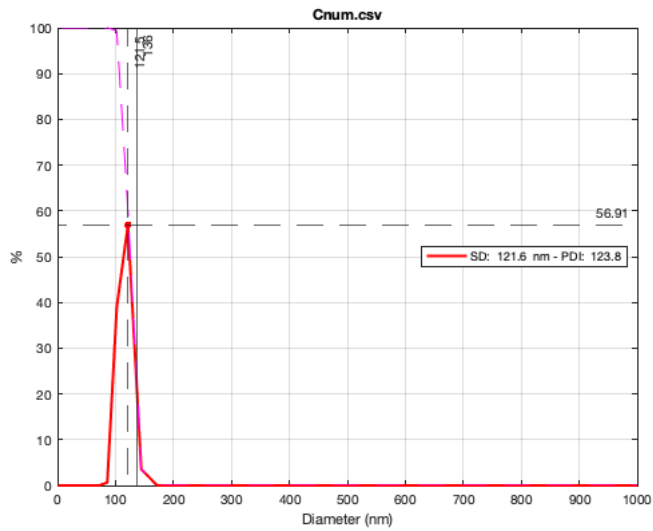
Plot

```
subplot(rw,1,i);
plot(data_t(:,1),data_t(:,2), LineWidth=2, Color=line_c)
hold on
plot(data_t(:,1),data_t(:,3), LineWidth=1, LineStyle="--", Color='m')
plot(data_t(my,1), mx, 'r.', MarkerSize=12)
xline(data_t(my,1), '--', data_t(my,1))
yline(mx, '--', mx)
xline(tables(part_median,3), '-', tables(part_median,3))
hold off
xlabel('Diameter (nm)')
```

```

ylabel('%')
title(names)
legend({join(['SD: ',string(tables(sd,3)),' nm - PDI: ', string(tables(pdi,3))]),Location='East'})
grid on
xlim([0,1000]) % range of size nm

```



Particle concentration in the samples

```

pv = v(data_t(:,1).*1e-7).*data_t(:,2)./100; % volume of nanoparticle
Np = round((massE./dsio2)./nonzeros(pv)); % number of particles in solution
pdens = Np./vf; % density of the particles in particles/liter
table([nonzeros(data_t(:,1)).*(data_t(:,2)~=0)],[pdens], VariableNames = {'particle diameter (nm)','particle density (particles/L)'} % print the t
fprintf('Cumulative particle density (particles/L): %3.2e \n',sum(pdens));

```

ans =

4×2 table

particle diameter (nm)	particle density (particles/L)
144.5	1.5488e+16
121.5	1.6161e+15
102.2	3.9736e+15
85.9	3.8844e+17

Cumulative particle density (particles/L): 4.10e+17

```

end
sgtitle(figName)

```

ExtractFluorescence.m

Created by: Alessandro Ascani Orsini

Date: 1/21/2023

Description: This code selects the fluorescence data in a file, plots it and extracts the peaks, in excel.

Contents

- [Clean everything](#)
- [Settings](#)
- [Import the data](#)
- [Plot fluorescence and max spectrum](#)
- [Blank subtract](#)

Clean everything

```
close all;
clear all;
clc;
```

Settings

```
file_n = 'fl 2-23-23.txt'; % name of the file
c = 12; % columns used on the slate
exp_em = 525; % check emission at a certain wl in nm
exp_ex = 470; % excitation
```

Import the data

```
fl_raw = readcell(file_n); % extract the data row
for i = 3:length(fl_raw)
    fl_raw{i} = str2double(strsplit(fl_raw{i}));
end
i = 0; % reset counter
for h = 3:length(fl_raw)
    if length(fl_raw{h})>c
        i = 1+i; % go to the next matrix
        j = 1; % set the new row of the matrix
        wl(h) = fl_raw{h}(1); % get the wavelength
        flmat(j,:,i) = fl_raw{h}(3:end); % select only values of interest
    else
        wl(h) = wl(h-1); % update the wavelength
        flmat(j,:,i) = fl_raw{h}(1:end); % put the whole thing in
    end
    j = j+1; % increase count
end
wl = nonzeros(unique(wl)); % clean the wl array
```

Plot fluorescence and max spectrum

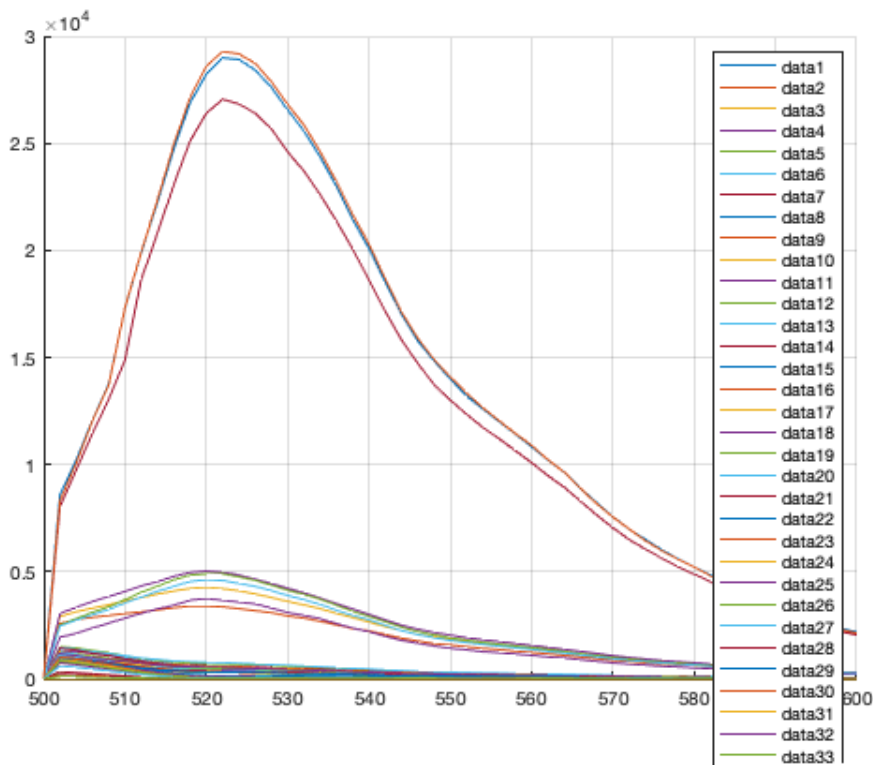
```
max_fl = zeros(size(flmat,1),size(flmat,2));
max_wl = max_fl;
```

```

exp_fl = max_fl;
figure()
hold on
for i = 1:size(flmat,1)
    for j =1:size(flmat,2)
        spectrum = flmat(i,j,:); % plot the spectrum
        [max_fl(i,j),max_wl(i,j)] = max(nonzeros((wl>exp_ex).*spectrum(:))); % extract max emission
        if isempty(nonzeros((wl==exp_em).*(spectrum(:))))
            exp_fl(i,j) = 0;
        else
            exp_fl(i,j) = nonzeros((wl==exp_em).*(spectrum(:))); % extract emission at designed wavelength
        end
        plot(wl(:),spectrum(:).*(wl>exp_ex))
    end
end
max_wl = wl(max_wl+length(nonzeros((wl<exp_ex))));
grid on
legend
hold off

```

Warning: Limiting legend entries to 50. Specify a vector of graphics objects to display more than 50 entries.



Blank subtract

```

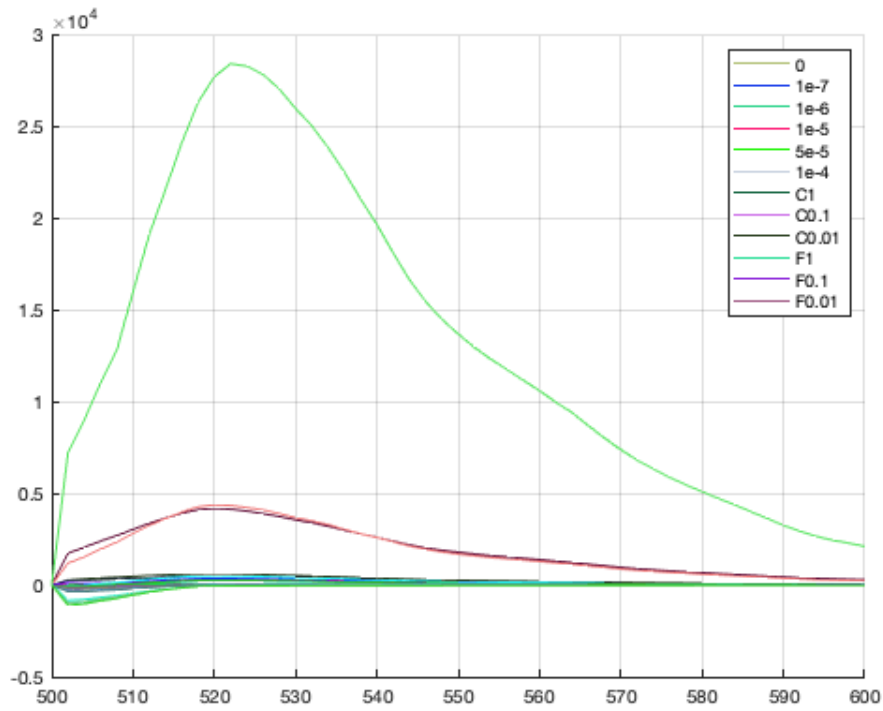
bl_avg = mean(flmat(1,1:3,:)); % take the mean of the blanks
bl_sub = flmat-bl_avg; % subtract the blanks average from each
st_avg = mean(bl_sub(:,1:3,:),2); % average of standards
sa_avg = [mean(bl_sub(:,4:6,:),2),mean(bl_sub(:,7:9,:),2),mean(bl_sub(:,10:12,:),2)]; % average of samples
a=[st_avg,sa_avg];
amax = max(a,[],3); % max matrix
figure()
hold on

```

```

for i = 1:size(a,1)
    for j =1:size(a,2)
        spectrum = a(i,j,:);
        plot(wl(:),spectrum(:).*(wl>exp_ex),Color = rand(1,3))
    end
end
grid on
legend('0','1e-7','1e-6','1e-5','5e-5','1e-4','C1','C0.1','C0.01','F1','F0.1','F0.01')
hold off

```



Bibliography

- [1] Daniela Pietrobon and Michael A Moskowitz. Chaos and commotion in the wake of cortical spreading depression and spreading depolarizations. 15(June), 2014.
- [2] R. Gangarosa. Utilizing fiber fluorescence for oxygen sensing in living tissue. 2022.
- [3] Eric R. Kandel, James H. Schwartz, Thomas M. Jessell, Steven A. Siegelbaum, and A. J. Hudspeth. *Principles of Neural Science, Fifth Edition*. McGraw-Hill Education / Medical, 5th edition, 2012.
- [4] Epilepsy Foundation. What is epilepsy?, n.d. Accessed on 2023-02-12.
- [5] CDC. Epilepsy, October 25 2022. Retrieved on December 2nd, 2022.
- [6] A. A. P. Leao. Spreading depression of activity in the cerebral cortex. *Journal of Neurophysiology*, 7(6):359–390, 1944.
- [7] George G Somjen. Mechanisms of spreading depression and hypoxic spreading depression-like depolarization. *Physiological reviews*, 81(3):1065–1096, 2001.
- [8] J. Liu and B. Gluckman. Tissue oxygenation dynamics during seizure to spreading depression transition in rat brain. Master’s thesis, The Pennsylvania State University, 2021.
- [9] AL Hodgkin and AF Huxley. A quantitative description of membrane current and its application to conduction and excitation in nerve. *Journal of Physiology*, 117(4):500–544, Aug 1952.
- [10] J. M. Ingram, C. Zhang, J. Xu, and S. J. Schiff. Fret excited ratiometric oxygensensing in living tissue. *Journal of Neuroscience Methods*, 214(1):45–51, 2013.
- [11] S. Gavriluk, S. Polyutov, P. C. Jha, Z. Rinkevicius, H. Ågren, and F. Gel’mukhanov. Many-photon dynamics of photobleaching. *The Journal of Physical Chemistry A*, 111(47):11961–11975, 2007.
- [12] Jinhyang Choi, Andrew A. Burns, Rebecca M. Williams, Zongziang Zhou, Andrea Flesken-Nikitin, Warren R. Zipfel, Ulrich Wiesner, and Alexander Y. Nikitin. Core-shell silica nanoparticles as fluorescent labels for nanomedicine. *Journal of Biomedical Optics*, 12(06):1, 2008.

- [13] Evan Phillips, Oula Penate-Medina, Pat B. Zanzonico, Richard D. Carvajal, Pauliah Mohan, Yunpeng Ye, John Humm, Mithat Gönen, Hovanes Kalaigian, Heiko Schöder, H. William Strauss, Steven M. Larson, Ulrich Wiesner, and Michelle S. Bradbury. Clinical translation of an ultrasmall inorganic optical-PET imaging nanoparticle probe. *Science Translational Medicine*, 6(260):1–10, 2014.
- [14] Chuanliu Wu, Jinqing Hong, Xiangqun Guo, Chaobiao Huang, Jinping Lai, Jinsheng Zheng, Jianbin Chen, Xue Mu, and Yibing Zhao. Fluorescent core-shell silica nanoparticles as tunable precursors: Towards encoding and multifunctional nano-probes. *Chemical Communications*, (6):750–752, 2008.
- [15] A. M. Nuruzatulifah, A. A. Nizam, and N. M. Nasha Ain. Synthesis and Characterization of Polystyrene Nanoparticles with Covalently Attached Fluorescent Dye. *Materials Today: Proceedings*, 3(Icfmd 2015):S112–S119, 2016.
- [16] Xu Dong Wang, Daniela E. Achatz, Christina Hupf, Michaela Sperber, Joachim Wegener, Sebastian Bange, John M. Lupton, and Otto S. Wolfbeis. Imaging of cellular oxygen via two-photon excitation of fluorescent sensor nanoparticles. *Sensors and Actuators, B: Chemical*, 188:257–262, 2013.
- [17] Davies and Bin Tian and James L. Manley. NIH Public Access. *Bone*, 23(1):1–7, 2008.
- [18] Heather A. Clark, Susan L.R. Barker, Murphy Brasuel, Michael T. Miller, Eric Monson, Steve Parus, Zhong You Shi, Antonius Song, Bjorn Thorsrud, Raoul Kopelman, Alex Ade, Walter Meixner, Brian Athey, Marion Hoyer, Dwayne Hill, Rhonda Lightle, and Martin A. Philbert. Subcellular optochemical nanobiosensors: Probes encapsulated by biologically localised embedding (PEBBLEs). *Sensors and Actuators, B: Chemical*, 51(1-3):12–16, 1998.
- [19] Timothy T Morgan, Hari S Muddana, Engin I Altinoglu, Sarah M Rouse, Amra Tabaković, Tristan Tabouillot, Thomas J Russin, Sivaprakash S Shanmugavelandy, Peter J Butler, Peter C Eklund, Jong K Yun, Mark Kester, and James H Adair. Encapsulation of organic molecules in calcium phosphate nanocomposite particles for intracellular imaging and drug delivery. *Nano letters*, 8(12):4108–4115, 2008.
- [20] Joseph R. Lakowicz. *Principles of fluorescence spectroscopy*. 2006.
- [21] Libretexts. 10.3.1: Intrinsic and extrinsic fluorophores, Aug 2022.
- [22] Michela Quaranta, Sergey M. Borisov, and Ingo Klimant. Indicators for optical oxygen sensors. *Bioanalytical Reviews*, 4(2-4):115–157, 2012.
- [23] Mojtaba Shamsipur, Ali Barati, and Ziba Nematifar. Fluorescent pH nanosensors: Design strategies and applications. *Journal of Photochemistry and Photobiology C: Photochemistry Reviews*, 39:76–141, 2019.

- [24] Xu Dong Wang and Otto S. Wolfbeis. Optical methods for sensing and imaging oxygen: Materials, spectroscopies and applications. *Chemical Society Reviews*, 43(10):3666–3761, 2014.
- [25] Joel Wellbourne-Wood, Theresa S. Rimmelé, and Jean-Yves Chatton. Imaging extracellular potassium dynamics in brain tissue using a potassium-sensitive nanosensor. *Neurophotonics*, 4(1):015002, 2017.
- [26] Fujimoto. NIH Public Access. *Bone*, 23(1):1–7, 2008.
- [27] W. Stöber, A. Fink, and E. Bohn. Controlled growth of monodisperse silica spheres in the micron size range. *Journal of Colloid and Interface Science*, 26(1):62–69, 1968.
- [28] Jonathan M Hughes, Peter M Budd, Andrew Grieve, Pranab Dutta, Karen Tiede, and John Lewis. Highly monodisperse, lanthanide-containing polystyrene nanoparticles as potential standard reference materials for environmental “nano” fate analysis. *Journal of Applied Polymer Science*, 132(24), 2015.
- [29] C. Jeffrey Brinker and George W. Scherer. *Sol-Gel Science: The Physics and Chemistry of Sol-Gel Processing*, 2013.
- [30] JH Adair, T Nagira, CM Brown, SR Khan, and WC Thomas Jr. Heterogeneous deposition of calcium phosphates at the silicon (hydrous) oxide-water interface. In R Ryall, R Bais, VR Marshall, AM Rofe, LH Smith, and VR Walker, editors, *Urolithiasis 2*, pages 181–187, New York, NY, 1995. Plenum Press.
- [31] Hari S. Muddana, Thomas T. Morgan, James H. Adair, and Peter J. Butler. Photophysics of Cy3-encapsulated calcium phosphate nanoparticles. *Nano Letters*, 9(4):1559–1566, 2009.
- [32] David W. Moore and Clyde Orr. The influence of diffusion on sedimentational particle size analysis. *Powder Technology*, 8(1-2):13–17, 1973.
- [33] International Organization for Standardization. ISO 15901-2:2022 - pore size distribution and porosity of solid materials by mercury porosimetry and gas adsorption — part 2: Analysis of nanopores by gas adsorption, 2022. Accessed on March 6, 2023.
- [34] Polymer Database. Orthosilicates. <https://polymerdatabase.com/Polymer> [Accessed: March 7, 2023].